

# The Multiverse, the Milky Universe, and the Periodic Table of Elementary Particles

Ding-Yu Chung\*

The basic components in the universe are space-time dimension numbers (from 4 to 11), object types (membrane, string, particle, and particle-wave), and space types (femion space for fermion, boson space for boson, and other spaces). In the multiverse, different universes have different dimensional numbers, object types, and space types. With different space-time number and object-space, the hidden universe is hidden and parallel to our observable universe. When the hidden universe with  $> 4$ D space-time becomes 4D space-time as the observable universe, it becomes dark energy in the observable universe. Derived from space-time dimension number (from 4 to 11) to define space-time, mass dimension number (from 4 to 11) defines mass. With different mass dimension numbers, dark matter is invisible and incompatible to baryonic matter. Incompatible dark matter and baryonic matter generate the milky universe, consisting of the inhomogeneous structures, such as galaxies and clusters. Mass dimensions also lead to seven dimensional orbitals in the observable universe. (Seven dimensional orbitals come indirectly from the seven extra dimensions in eleven-dimensional space-time.) The three sets of seven dimensional orbitals establish the periodic table of elementary particles for all gauge bosons, leptons and quarks, and explain the composition of hadrons. The calculated masses for elementary particles and hadrons are in good agreement with the observed masses. For examples, the calculated masses for the top quark, neutron, and pion are 176.5 GeV, 939.54MeV, and 135.01MeV in excellent agreement with the observed masses,  $174.3 \pm 5.1$ GeV, 939.57 MeV, and 134.98 MeV, respectively.

## Introduction

All leptons, quarks, and gauge bosons can be placed in the periodic table of elementary particles [1]. As the periodic table of elements derived from atomic orbital, the periodic table of elementary particles is derived from the two sets of seven orbitals: principal dimensional orbital and auxiliary dimensional orbital. (Seven orbitals come indirectly from the seven extra dimensions in eleven-dimensional space-time.) Principal dimensional orbital explains gauge boson and low-mass leptons, and auxiliary dimensional orbital accounts for high-mass leptons and quarks. The first indication of orbital structure for elementary particle appeared in the quantized lepton mass formula by A.O. Barut [2].

$$M_n = M_e + \frac{3M_e}{2\alpha} \sum_{n=0}^n n^4$$

where  $n = 0, 1$ , and  $2$  for electron, muon, and  $\tau$ , respectively. The calculated masses  $105.5$  and  $1786$  MeV for muon and  $\tau$ , respectively, in good agreement with the observed masses,  $105.7$  and  $1777$  MeV. The quantized lepton mass formula indicates the orbital structure. The periodic table of elementary particles bases on the Barut lepton mass formula.

Furthermore, there is third set of seven orbitals for hadrons [3], the composites of quarks. The three sets of seven orbitals relate to MacGregor-Akers constituent quark model [4], whose calculated masses of hadrons are in good agreement with the observed values.

The paper proposes that seven orbitals indirectly come from seven extra space-time dimensions of eleven-dimensional space-time. The first two sets of seven orbitals comes from the combination of the two eleven dimensional universes, implying the multiverse. In the multiverse, different universes have different space-time dimension numbers (from  $4$  to  $11$ ), different object types (membrane, string, particle, and particle-wave), and different space types (fermion space for fermion, boson space for boson, and other spaces). This paper proposes varying dimension number and varying object-space in the multiverse.

The paper is divided into three parts: the multiverse, the Milky Universe, and the periodic table of elementary particles. Section 1 describes varying space-time dimensions and varying mass dimensions. Section 2 describes the evolution of the expanding universe and object-space. The cosmic expansion mechanism and the two different modes of the cosmic expansion are described in Section 3. In Section 4, the cyclic universe is proposed. The formation of inhomogenous structure in the observable universe based on the Milky Universe is described in Section 5. The evolution of galaxies is stated in Section 6. Section 7 is about high-energy cosmic rays. In Sections 8, 9, 10, and 11, the periodic table of elementary particles is constructed to account of all leptons, quarks, gauge bosons, and hadrons, QCD, and their masses are calculated.

## Part 1: The Multiverse

### 1. The Varying Dimension Number

The multiverse consists of two variable components: varying dimension number and varying object-space. Different universes in the multiverse have different compositions of variables from the two variable components.

Varying dimension numbers are derived from varying speed of light (VSL) theory [5]. The constancy of the speed of light is the pillar of special relativity. The constancy of the speed of light takes place in the four dimensional space-time whose space-time dimension number (four) is constant. In the varying speed of light (VSL) model [6] of cosmology by Albrecht, Magueijo, and Barrow, the speed of light varies in time. The time dependent speed of light varies as some power of the expansion scale factor,  $a$ , in such way that

$$c(t) = c_0 a^n \quad (1)$$

where  $c_0 > 0$  and  $n$  are constant. The increase of speed of light is continuous.

This paper posits quantized varying speed of light (QVSL), where the speed of light is invariant in a constant space-time dimension number, and the speed of light varies with varying space-time dimension number from 4 to 11. In QVSL, the speed of light is quantized by varying space-time dimension number.

$$c_D = c / \alpha^{D-4}, \quad (2)$$

where  $c$  is the observed speed of light in the 4D space-time,  $c_D$  is the quantized varying speed of light in space-time dimension number,  $D$ , from 4 to 11, and  $\alpha$  is the fine structure constant. Each dimensional space-time has a specific speed of light. The speed of light increases with increasing space-time dimension number,  $D$ . In the VDN model of cosmology, the universe starts with the pre-expanding universe that has the speed of light in 11D space-time.

In special relativity,  $E = M_0 c^2$  modified by eq. (2) is expressed as

$$E = M_0 (c^2 / \alpha^{2(D-4)}) \quad (3a)$$

$$= (M_0 / \alpha^{2(d-4)}) c^2 \quad (3b)$$

Eq. (3a) means that a particle in the  $D$  dimensional space-time can have superluminal speed,  $c / \alpha^{D-4}$ , that is higher than the observed speed of light, and has rest mass,  $M_0$ . Eq. (3b) means that the same particle in the 4D space-time with the observed speed of light acquires  $M_0 / \alpha^{2(d-4)}$  as the rest mass where  $d = D$ .  $D$  in eq. (3a) is space-time dimension number defining the varying speed of light. In eq. (3b),  $d$  from 4 to 11 is “mass dimension number” defining varying mass. For example, for  $D = 11$ , eq. (3a) shows a superluminal particle in eleven-dimensional space-time, while eq. (3b) shows that the speed of light of the same particle is the observed speed of light with the 4D space-time, and the mass dimension is eleven. In other words, 11D space-time can transform into 4D space-time with 11d mass dimension. QVSL in terms of varying space-time dimension number,  $D$ , brings about varying mass in terms of varying mass dimension number,  $d$ .

The QVSL transformation transforms space-time dimension number and mass dimension number. In the QVSL transformation, the decrease in the speed of light leads to the decrease in space-time dimension number and the increase of mass in terms of increasing mass dimension number from 4 to 11.

$$c_D = c_{D-n} / \alpha^{2n}, \quad (4a)$$

$$M_{0,D,d} = M_{0,D-n,d+n} \alpha^{2n}, \quad (4b)$$

$$D, d \xrightarrow{QVSL} (D \mp n), (d \pm n) \quad (4c)$$

where  $D$  is space-time dimension number from 4 to 11 and  $d$  is mass dimension number from 4 to 11. For example, the QVSL transformation transforms a particle with 11D4d to a

particle with 4D11d. In terms of rest mass, 11D space-time has 4d with the lowest rest mass, and 4D space-time has 11d with the highest rest mass.

The QVSL transformation is an alternate to the Higgs mechanism to gain rest mass. In the QVSL, the speed of light is constant in a specific space-time dimension number, such as 4 for our four-dimensional space-time. In different space-time dimension numbers (from 4 to 11), speeds of light are different. In our four-dimensional space-time, the speed of light is the lowest, so according to special relativity ( $E = m_0c^2$ ), with constant energy, the rest mass in our four-dimensional space-time is the highest. Thus, instead of absorbing the Higgs boson to gain rest mass, a particle can gain rest mass by decreasing the speed of light and space-time dimension number. The QVSL transformation also gain a new quantum number, “mass dimension number” from 4 to 11 to explain the hierarchical masses of elementary particles. Since the Higgs bosons have not been found experimentally, the QVSL transformation to gain rest mass is a good alternate. In terms of vacuum energy, the four-dimensional space-time has zero vacuum energy with the highest rest mass, while  $D > 4$  have non-zero vacuum energy with lower rest mass than 4D.

Since the speed of light for  $> 4D$  particle is greater than the speed of light for 4D particle, the observation of  $> 4D$  particles by 4D particles violates causality. Thus,  $> 4D$  particles are hidden particles with respect to 4D particles. Such hidden particles form the base for phantom energy [7] and the hidden universe.

In the normal supersymmetry transformation, the repeated application of the fermion-boson transformation transforms a boson (or fermion) from one point to the same boson (or fermion) at another point at the same mass. In the “varying supersymmetry transformation”, the repeated application of the fermion-boson transformation transforms a boson from one point to the boson at another point at different mass dimension number in the same space-time number. The repeated varying supersymmetry transformation transforms boson  $B_d$  into fermion  $F_d$  and from fermion  $F_d$  to boson  $B_{d-1}$  is expressed as

$$M_{d, F} = M_{d, B} \alpha_{d, B}, \quad (5a)$$

$$M_{d-1, B} = M_{d, F} \alpha_{d, F}, \quad (5b)$$

where  $M_{d, B}$  and  $M_{d, F}$  are the masses for a boson and a fermion, respectively,  $d$  is mass dimension number, and  $\alpha_{d, B}$  or  $\alpha_{d, F}$  is the fine structure constant, which is the ratio between the masses of a boson and its fermionic partner. Assuming  $\alpha_{d, B} = \alpha_{d, F}$ , the relation between the bosons in the adjacent dimensions, then, can be expressed as

$$M_{d-1, B} = M_{d, B} \alpha_d^2, \quad (5c)$$

Eq. 5 shows that it is possible to describe mass dimensions  $> 4$  in terms of

$$F_5 B_5 F_6 B_6 F_7 B_7 F_8 B_8 F_9 B_9 F_{10} B_{10} F_{11} B_{11} \quad , \quad (6)$$

where the energy of  $B_{11}$  is Planck energy. Each mass dimension between 4d and 11d consists of a boson and a fermion. Eq. 5 shows a stepwise transformation that transforms a particle with d mass dimension to  $d \pm 1$  mass dimension. The transformation from higher dimensional particle to adjacent lower dimensional particle is the fractionalization of a higher dimensional particle to many lower dimensional particle in such way the number of lower dimensional particles  $= n_{d-1} = n_d / \alpha^2$ . The transformation from lower dimensional particles to higher dimensional particle is condensation. Both the fractionalization and the condensation are stepwise. For example, a particle with 4D (space-time)10d (mass dimension) can transform stepwise into 4D9d particles. Since supersymmetry transformation involves translation, this stepwise varying supersymmetry transformation leads to translational fractionalization and translational condensation, resulting in expansion and contraction.

Another type of the varying supersymmetry transformation is not stepwise. It is the leaping varying supersymmetry transformation that transforms a particle with d mass dimension to any  $d \pm n$  mass dimension. The transformation involves the fission-fusion of particle. The transformation from d to  $d - n$  involves the fission of a particle with d mass dimension into two parts: the core particle with  $d - n$  dimension and the dimensional orbitals that are separable from the core particle. (Section 3 will deals with the mechanism of the fission.) The sum of the number of mass dimensions for a particle and the number of dimensional orbitals is equal to 11 for all particles with mass dimensions. Therefore,

$$F_d = F_{d-n} + (11-d+n) DO's , \quad (7)$$

where  $11 - d + n$  is the number of dimensional orbitals (DO's) for  $F_{d-n}$ . For example, the fission of 4D9d particle produces 4D4d particle that has  $d = 4$  core particle and 7 separable dimensional orbitals in the form of  $B_5F_5B_6F_6B_7F_7B_8F_8B_9F_9B_{10}F_{10}B_{11}$ . Since the fission process is not stepwise from higher mass dimension to lower mass dimension, it is possible to have simultaneous fission. For example, 4D9d particles can simultaneously transform into 4D8d, 4D7d, 4D6d, 4D5d, and 4D4d particles, which have 3, 4, 5, 6, and 7 separable dimensional orbitals, respectively. Therefore, varying supersymmetry transformation can be stepwise or leaping. Stepwise supersymmetry transformation is translational fractionalization and condensation, resulting in stepwise expansion and contraction. Leaping supersymmetry transformation is not translational, and it is fission and fusion, resulting possibly in simultaneous formation of different particles with separable dimensional orbitals.

In summary, the QVSL transformation transform space-time dimension number and mass dimension number. The varying supersymmetry transforms varying mass dimension number in the same space-time number as follows (D = space-time dimension number and d = mass dimension number).

$$D, d \xrightarrow{QVSL} (D \mp n), (d \pm n)$$

$$D, d \xrightarrow{\text{stepwise or leaping varying supersymmetry}} D, (d \pm 1) \text{ or } D, (d \pm n)$$

## 2. *From the Pre-universe to the Expanding Universe: Variable Object-Space*

Another variable component of the multiverse is object-space component consisting of four objects and four spaces. Objects has definite shapes, and spaces are homogeneous. Objects include string, membrane, particle, and particle-wave. Spaces include blank space, fermion space, boson space, and detachment space. Blank space takes turn to coexist equally with object at the same location as in creation and annihilation of particle in vacuum. Fermion space exists with an object at the same location or different locations in one object to one space relation as in fermion. Boson space exists at the same location with multiple objects as in boson. Detachment space detaches particle from its position.

The evolution of our expanding universe involves four stages: the pre-universe, the pre-expanding universe, the mixed pre-expanding universe, and the expanding universe. Different stages of evolution have different compositions of variables from varying space-time dimensions and varying object-space.

The starting multiverse (the pre-universe) is essentially a homogeneous blank consisting of 10D superstring in equilibrium with vacuum at a non-zero vacuum energy and superluminal speed. The pre-universe is blank space-object, the equilibrium state between the vacuum and the pairs of ten-dimensional superstring and anti-superstring. The vacuum energy is equal to the non-zero energy of the superstring. The pre-universe is the platform for the multiverse.

Blank space can also undergoes vacuum fluctuation as condensation and diffusion. The condensation as the compactification of higher dimensions leads to the formation of a two space-time dimensional string and the empty space as fermion space, each of which associates with one object. One object per space is the definition of fermion.

The compact two space-time dimensional string has the Planck mass. This 2D string attaches to the 10D superstring to provide the eleventh dimension for an eleven-dimensional membrane as Fig. (1). The compact string has the Planck mass. The pre-universe is pre-quantum mechanics without uncertainty, so without uncertainty, the space-time of the 2D-string attaches to the space-time of the adjacent 10D-superstring precisely. This evolution from string to membrane is the reverse of M-theory that starts with 11D-membrane.

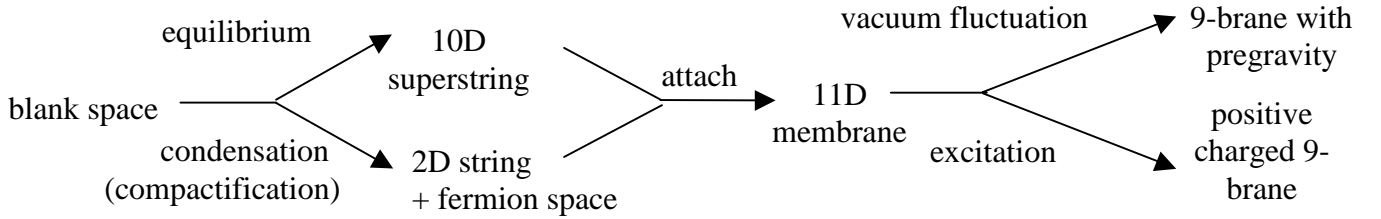


**Fig. 1:** the evolution of 9-brane in the pre-expanding universe

The attached string can undergo vacuum fluctuation and excitation. In terms of vacuum fluctuation, the non-zero vacuum energy causes the attached string to diffuse into fermion space to become an infinite dimension. Subsequently, the attachment of the string in membrane provides AdS (anti-de Sitter space) for the diffused string to condense (compactify) again. When this diffusion-condensation overlaps with the diffusion-condensation from another membrane, "pregravity" (the predecessor of gravity) is formed. Pregravity is in boson space that allows more than multiple objects per space. Boson is defined as multiple objects per space. This diffusion-condensation reproduces the Planck-infinite dimension in the Randall-Sundrum model [8] for gravity. The resulting structure is 9-brane (10D-brane) embedded in the eleven-dimensional bulk with pregravity. Since pregravity is active in an empty space, pregravity is a long-ranged force as Fig. 1 and Fig. 2.

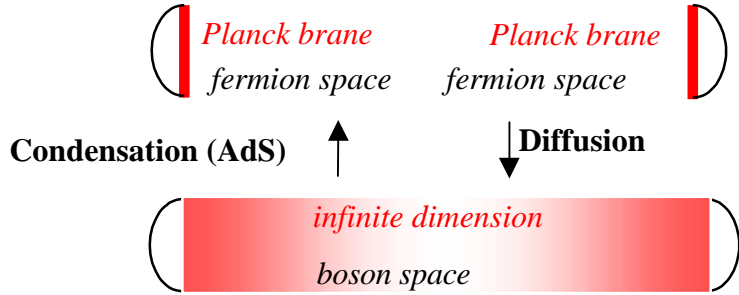


**Fig. 2:** pregravity as the Randall-Sundrum model

In terms of excitation, the attached string behaves as the 1D circle circling superstring in the 10D x 1D Kaluza-Klein structure. The quantized excitation of the circle brings about the quantized positive pre-charged force (the predecessor of electromagnetism) with the absorption and the emission of the massless particles in exchange with the massless particles from other membranes. Since the pre-charged force is active in empty space, the pre-charged force is a long-ranged force as Fig. 1 and Fig. 3.

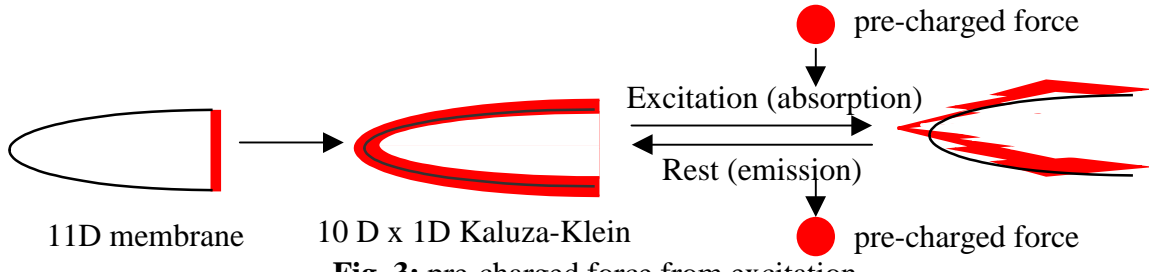


**Fig. 3:** pre-charged force from excitation

The combination of the vacuum fluctuation and the excitation of the attached string results in the positive charged 9-brane embedded in the eleven-dimensional bulk with pregravity and positive pre-charged force (Fig. 1). At the same time, the ten-dimensional anti-superstring becomes negative charged 9-antibrane embedded in the eleven-dimensional bulk with anti-pregravity and negative pre-charged force.

The original force among strings in the pre-universe is the pre-strong force, the predecessor of the strong force. The force is resulted from the absorption and the emission of massless particles from strings. Since it transmits through blank space with non-zero energy, rather than an empty space, it is a short-ranged force through a non-zero energy medium. This pre-strong force remains as a short-ranged force among membranes.

The combination of the 9-brane and the 9-antibrane is the brane-antibrane unit. The structure of the brane-antibrane unit is determined by the evolutionary sequence of the three forces. In the normal evolutionary sequence, the pre-strong force exists first. Then, the emergence of the repulsive force between pregravity and anti-pregravity forces a brane and an antibrane to move away from each other. Subsequently, the pre-strong force connects the newly formed brane or the antibrane with previously formed branes or antibranes. Finally, the pre-charged force emerges. The space occupied by branes is opposite from the space occupied by antibranes, so branes and antibranes are chiral. This normal evolutionary sequence provides the chiral brane-antibrane unit where the chiral boundary positive charged 9-brane and the chiral boundary negative charged 9-antibrane embedded in the eleven-dimensional space-time are separated by chiral pregravity and chiral anti-pregravity as Fig. 4.

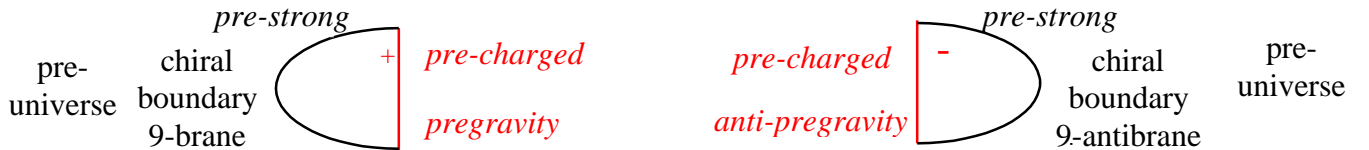


**Fig. 4:** the pre-expanding universe

The pre-expanding universe emerges with this chiral brane-antibrane unit as the predominant structure. All forces and membranes inside the pre-expanding universes are chiral. The pre-expanding universe continues to grow with the conversion of the pre-universe vacuum entering into the fermion space in the middle of the pre-expanding

universe. This two-brane structure of the pre-expanding universe also appears in the Horava-Witten eleven dimensional pregravity on a manifold with two ten-dimensional boundaries [9], the ekpyrotic universe boundary branes [10], and the brane-antibrane universe [11].

During the steady conversion from the pre-universe to the pre-expanding universe takes place, the total volume of the two universes remain constant. To maintain this constant volume, the attractive force ( $A$ ) between the positive and negative pre-charged forces is equal to the sum of the repulsive force ( $R$ ) between pregravity and anti-pregravity, and the special global short-ranged pre-strong force ( $C$ ) connecting the pre-expanding universe and the pre-universe.  $A = R + C$  is a non-localized global relation for the constant total volume of the universes. If  $A > R + C$ , the total volume is smaller, and if  $A < R + C$ , the total volume is larger.

There is a small amount of the abnormal evolutionary sequence in the pre-expanding universe. In the abnormal evolutionary sequence, the pre-strong force exists first. Then, the emergence of the attractive force from the pre-charged forces draws the brane and the antibrane together. The combined brane-antibrane units go impartially to either side of the pre-expanding universe, resulting in the achiral brane-antibrane units. (Essentially, attractive force and repulsive force are the tools to form chirality and achirality.) Finally, pregravity and anti-pregravity emerge. In the universe, local interactions are either chirality-specific or achirality-specific. Unable to interact with the region inside the chiral pre-expanding universe, the achiral brane-antibrane units are separated from the chiral pre-expanding universe, and congregate in the area connecting the pre-universe and the pre-expanding universe. The result is the decrease of the connection between the pre-expanding universe and the pre-universe. However, as a non-localized global relation,  $A = R + C$  continues with the right amount of  $C$  contributed by the pre-universe as long as there is still connection between the pre-universe and the pre-expanding universe.

As the pre-expanding universe grows with the chiral brane-antibrane units, the number of the achiral brane-antibrane units grows. Eventually, the pre-expanding universe is disconnected completely from the pre-universe by the achiral brane-antibrane units. Without  $C$ , the excess attractive force ( $A > R$ ) between positive branes and negative charged antibranes causes the pre-expanding universe to collapse, and the repulsive force between pregravity and anti-pregravity causes the pre-expanding universe to inverse. As the 9-brane and the 9-antibrane move toward each other, the 9-brane and the 9-antibrane turn inside, and pregravity and anti-pregravity turn outside. The "gulf" separating the pre-expanding universe and the pre-universe is formed. Eventually, the 9-brane and the 9-antibrane coalesce. At the end of the coalescence, the repulsion between pregravity and anti-pregravity causes a bounce after the collapse.

At this point, the complete coalescence leads to the loss of the properties of brane and antibrane in terms of the membrane property, the pre-charged force, the pre-strong force, and chirality. The result is the generation of the achiral mixed 9-particle with the multiple dimensional Kaluza-Klein structure without the requirements for identical space dimensions and a fixed number of space dimensions as in superstring. All forces formed previously become achiral. The bounce results in the mixed pre-expanding universe,

consisting of four equal parts: two groups of achiral mixed 9-particles, achiral pregravity, and achiral anti-pregravity as Fig. 5.

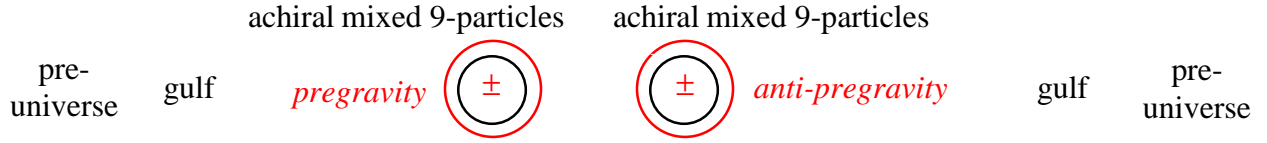


**Fig. 5:** the mixed pre-expanding universe

The interactions between branes in the form of collision are proposed in various brane models [10, 10]. The cyclic universe model based on the ekpyrotic universe [12] has the collapse-singularity-bounce scheme.

The size of the pre-expanding universe is determined by the ratio between the number of the chiral units and the number of the achiral units. The pre-universe and the mixed pre-expanding universe are different in the composition of objects and spaces, and are separated from each other permanently. Consequently, the two universes are completely transparent to each other. Without relation with the pre-universe, the mixed pre-expanding universe has its own vacuum energy that decreases from the non-zero in the pre-universe to zero. With decreasing vacuum energy and the Kaluza-Klein structure without a fixed number of space dimensions, the space-time dimension and the mass dimension of mixed 9-particles decrease to lower dimensional space-time and lower dimensional mass. The decrease to lower mass dimension results in the fractionalization of mixed 9-particles into lower mass particles, leading to the expansion of the universe. The fractionalization leads to the cosmic expansion into the completely transparent pre-universe. It is the start of the expanding universe. To the pre-universe, the expanding universe is a missing region.

### 3. *The Expanding Universe: the Hidden Universe and the Observable Universe*

The cosmic expansion in terms of the fractionalization of 9-mixed particles involves two different modes for the two sides of the expanding universe: the slow mode for the hidden universe and the quick mode for the observable universe.

In the slow mode, the vacuum energy decreases to zero gradually, and the space-time dimension of the 10D mixed particle with antigravity decreases from 10D to 4D, stepwise. In the hidden universe, the 10D4d particles at high vacuum energy transform into 9D5d particles at low vacuum energy through the QVSL transformation. Through the varying supersymmetry transformation, 9D5d becomes 9D4d. Such varying supersymmetry transformation brings about the stepwise translational fractionalization, resulting in cosmic expansion. Further decrease in vacuum energy repeats the same process again until particles are the 5D particles at low non-zero vacuum energy as follows.

$$10D4d \rightarrow 9D5d \rightarrow 9D4d \rightarrow 8D5d \rightarrow 8D4d \rightarrow 7D5d \rightarrow \bullet \bullet \bullet \rightarrow 5D4d$$

As mentioned before, since the speed of light for  $> 4D$  particle is greater than the speed of light for  $4D$  particle, the observation of  $> 4D$  particles by  $4D$  particles violates causality. Thus,  $> 4D$  particles are hidden particles with respect to  $4D$  particles. The universe with  $> 4D$  particles is the hidden universe.

The quick mode is used in the observable universe, which involves the inflation. Before the inflation, the universe is made of superstrings as  $10D4d$  with another dimension for gravity.  $10D4d$  superstring transforms through the QVSL transformation quickly into  $4D10d$  particles, which then transforms and fractionalizes quickly through varying supersymmetry transformation into  $4D9d$ , resulting in inflationary expansion [13]. The inflationary expansion occurs between the energy for  $4D10d = E_{\text{Planck}} \alpha^2 = 6 \times 10^{14} \text{ GeV}$  and the energy for  $4D9d = E_{10} \alpha^2 = 3 \times 10^{10} \text{ GeV}$ . At the end of the inflationary expansion, all  $4D9d$  particles undergo simultaneous fission to generate equally by mass and number into  $4D9d$ ,  $4D8d$ ,  $4D7d$ ,  $4D6d$ ,  $4D5d$ , and  $4D4d$  particles. Baryonic matter is  $4D4d$ , while dark matter consists of the other five types of particles. The mass ratio of dark matter to baryonic matter is 5 to 1 in agreement with the observation [14] that shows that the universe consists of 25% dark matter, 5% baryonic matter, and 70% dark energy. Afterward, quantum fluctuation and thermal expansion (the big bang) take place. In summary, the process is as follows.

$$\begin{array}{c}
 10D4d \xrightarrow{\text{QVSL transformation}} 4D10d \xrightarrow{\text{stepwise fractionalization, inflation}} \\
 4D9d \xrightarrow{\text{simultaneous fission}} 4D9d + 4D8d + 4D7d + 4D6d + 4D5d + 4D4d + \text{radiation} \\
 \rightarrow \text{quantum fluctuation + thermal cosmic expansion}
 \end{array}$$

The mechanism for the fission into core particle and dimensional orbital requires “detachment space” that detaches core particle and dimensional orbital. The physical source of detachment space comes from the empty space of the particle whose mass is detached. The particle as the mixed particle consists of internal brane and antibrane. With the CP symmetry, the particle has equal and opposite positive and negative charges for internal brane and antibrane, respectively, resulting annihilation (implosion). Annihilation is the detachment of energy from the original position. The empty space left behind the detachment is detachment space, and the detached energy is cosmic radiation. The particles with CP asymmetry remain as the particles (matter).

The absorption of detachment space in the gap between core particle and dimensional orbital initiates the fission. However, the gap between core particle and dimensional orbital is not purely detachment space that creates permanent detachment. The space between core particle and dimensional orbital is “hybrid space” from combining attachment space (the space for core particle) and detachment space. Hybrid space has neither complete attachment nor complete detachment. Hybrid space can be described by the uncertainty principle in quantum mechanics as

$$\Delta x \Delta p \geq h/4\pi, \quad (8)$$

where  $x$  is position and  $p$  is momentum. For the uncertainty principle in quantum mechanics,  $\Delta x$  is the uncertainty in position and  $\Delta p$  is the uncertainty in momentum during the measurement of the position and momentum of a particle. For hybrid space,  $\Delta x$  is distance of the gap between core particle and dimensional orbital, and  $\Delta p$  is the momentum in the gap from the by the contact between dimensional orbital and core particle.  $\Delta x \Delta p \geq h/4\pi$  shows that neither  $\Delta x$  nor  $\Delta p$  can be zero. Thus, there cannot be complete attachment where  $\Delta x = 0$ , and there cannot be complete detachment where  $\Delta p = 0$ . For hybrid space, the uncertainty principle without precise position and momentum becomes the gap principle without complete attachment and detachment.

The original purpose of hybrid space is for the microscopic gap between core particle and dimensional orbital, so hybrid space is microscopic. Thus, hybrid space as the space for all particles is microscopic. Hybrid space does not apply to macroscopic objects.  $\Delta x \Delta p \geq h/4\pi$  describes the probability of a particle in  $\Delta x$  and  $\Delta p$  in microscopic region. This probability is wavefunction. Particle becomes particle-wave.

The original purpose of hybrid space is for the gap in a coherent system of core particle and dimensional orbital, so hybrid space is coherent. Thus, hybrid space as the space for all particles is coherent. As in the theory of decoherence, any decoherence by the entanglement with decoherent system obliterates hybrid space, resulting in the collapse of wavefunction and the disappearance of  $\Delta x \Delta p \geq h/4\pi$ . With the gap principle, the microscopic nature, and the coherence, hybrid space for all particles is the space for quantum mechanics.

In summary for the cosmic evolution of object-space, the multiverse starts with the pre-universe that has string as object and blank space as space. The pre-expanding universe evolved from the pre-universe has membrane as object, and the additional spaces are fermion space for fermion and boson space for boson. The mixed pre-expanding universe evolved from the pre-expanding universe has particle as object. In the observable universe evolved from the mixed pre-expanding universe, the additional space is detachment space from the formation of cosmic radiation. Hybrid space from combining attachment space (fermion space and boson space) and detachment space forms the gap between core particle and dimensional orbital. Hybrid space also leads to particle-wave. The cosmic evolution of object-space is described in Fig. 6.

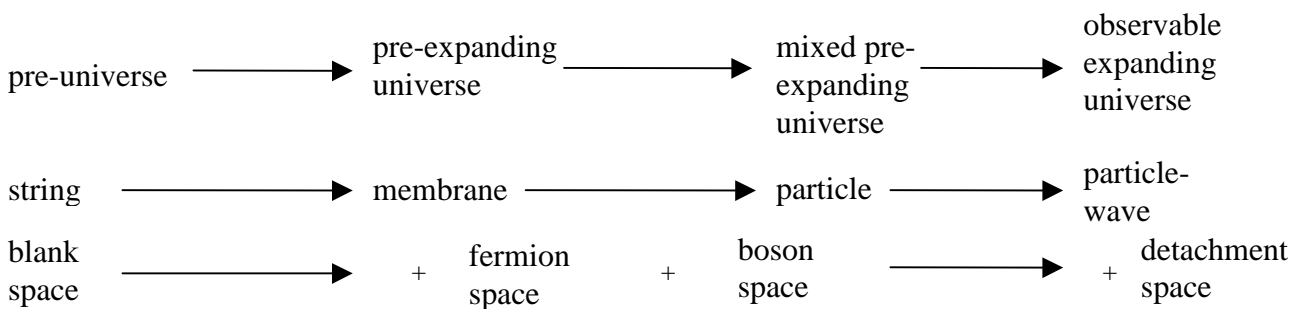


**Fig. 6:** the cosmic evolution of object-space

#### 4. *The Cyclic Universe*

The hidden universe with  $D > 4$  and the observable universe with  $D = 4$  are the “parallel universes” without any interaction between them. When the slow QVSL transformation of 5D hidden particles in the hidden universe into observable 4D particles, the observable 4D particles become the dark energy for the observable universe.

Physically, the observable universe gradually “swallows” the hidden universe including its energy density and negative pressure from anti-gravity, resulting in accelerated cosmic expansion. At a certain time, the hidden universe disappears, and becomes completely observable as dark energy. Afterward, 4D dark energy transforms back to  $> 4$ D particles that are not observable. The removal of dark energy in the observable universe leads to the removal of energy density and negative pressure, resulting in the stop of accelerated expansion and the start of contraction of the observable universe.

The end of dark energy starts another “parallel universe period” without any interaction between them. Both hidden universe and observable universe contract synchronically. Eventually, gravity causes the observable universe to crush to lose all cosmic radiation, resulting in the return to 4D9d particles, which then undergoes the deflation to become 4D10d particles. The increase in vacuum energy allows 4D10d particles to become 10D4d particles. Meanwhile, hidden  $> 4$ D particles in the hidden universe transform into 10D particles. Both universes return to the start of the cyclic universe, and start another cycle of the universe.

This two-universe model appears also in the two-universe (visible and hidden) model in the cyclic ekpyrotic universe model [12]. Fig. 7 shows the cyclic universe.

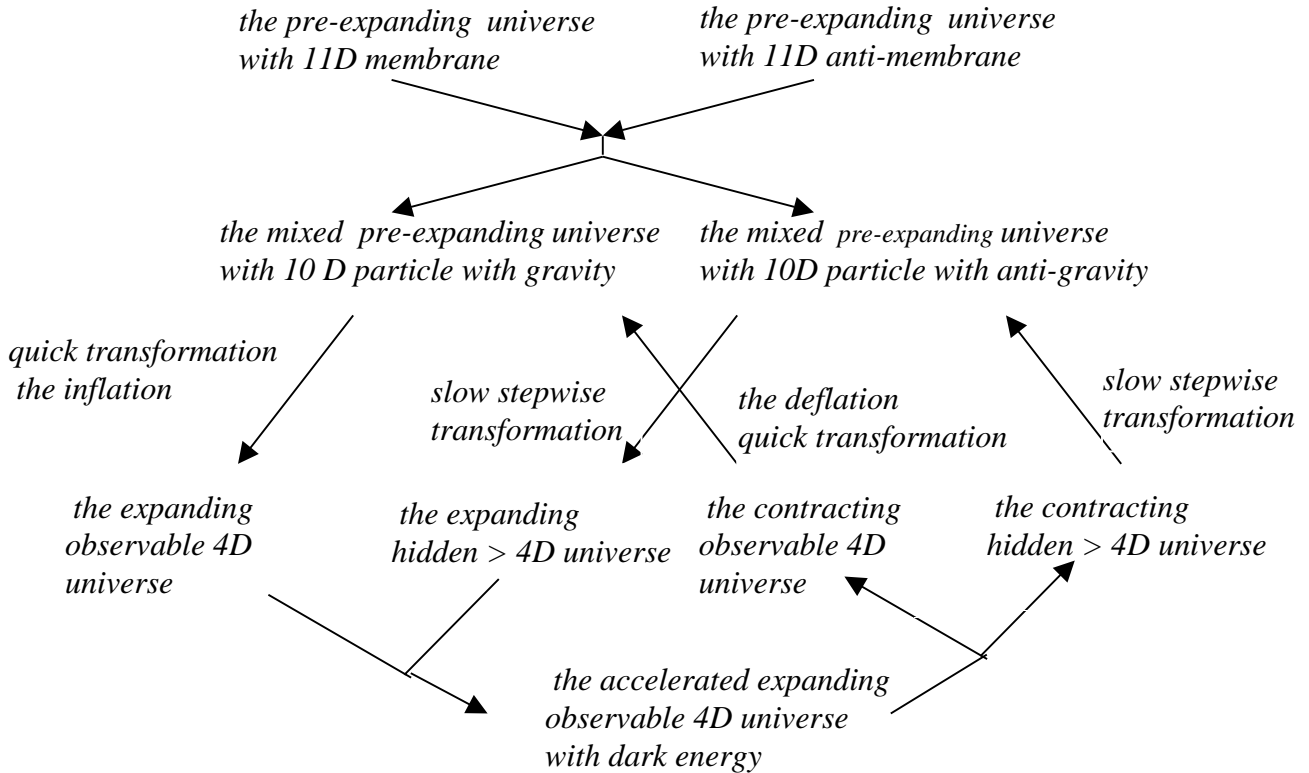


**Fig. 7:** the cyclic universe

## Part 2: The Milky Universe

### 5. The Formation of Inhomogeneous Structure

The second part of the cosmic evolution is the Milky Universe, where the inhomogeneous structures come from the incompatibility between baryonic matter and dark matter.

The observable universe consists of baryonic matter and dark matter. The baryonic matter has the 4-dimensional mass. Dark matter consists of five types of particles with mass dimensions from 5d to 9d. Both dark matter and baryonic matter share the same long-ranged gravity. As shown later, dark matter does not have electromagnetism, so it cannot be seen, but it can be observed by gravity. Such difference in electromagnetism results in the mass dimensional incompatibility between baryonic matter and dark matter. There are five types of particles from 4d to 9d. Baryonic matter is one of the six types of particles at equal mass proportions, so the baryonic mass fraction is 1/6. The calculated value agrees well with the observed value [14].

The Inflationary Universe scenario [13] provides possible solutions of the horizon, flatness and formation of structure problems. In the standard inflation theory, quantum fluctuations during the inflation are stretched exponentially so that they can become the seeds for the formation of inhomogeneous structure such as galaxies and galaxy clusters. They also produce anisotropies in CMB (cosmic microwave background). However, without fine-tuning, the calculated amplitude of the density perturbation induced by quantum fluctuations during the inflation is much larger than the observed amplitude in CMB. The small density perturbation is a serious problem in the inflation theory [15].

This paper posits that the inhomogeneous structure comes from mostly the incompatibility between dark matter and baryonic matter after the inflation. The space for quantum mechanics is hybrid space formed after the inflation, so quantum fluctuation plays minor role for the inhomogeneous structure. The inhomogeneous structure is analogous to emulsion (such as milk) by the incompatibility between two materials such as oil and water. (The incompatibility between oil and water is due to electromagnetic property in terms of polarity.) Cosmic radiation is compatible with both baryonic matter and dark matter through the commonality in detachment space. The incompatibility between baryonic matter and dark matter increases linearly with decreasing temperature of cosmic radiation whose temperature decreases with increasing size of the universe. Thus, the incompatibility increases with increasing size of the universe. The whole universe behaves as one unit of emulsion. In emulsion, oil exists as free oil among water or as oil in oil droplet. Similarly, baryonic matter exists as free baryonic matter among dark matter or as baryonic matter in the baryonic droplet.

At the beginning of the expanding universe after the inflation and the fission, with high cosmic radiation density, baryonic matter and dark matter were completely compatible with each other, and baryonic matter existed entirely as free baryonic matter. At the time of the recombination, the inhomogeneous structure by the incompatibility between dark matter and baryonic matter causes small-scale variant in terms of inhomogeneous structure as observed recently [16] by the presence of small amount of baryonic matter droplet. As the universe expanded after the time of recombination, the density of cosmic radiation decreases, and the size of the baryonic droplets increased with the increasing incompatibility between baryonic matter and dark matter. The growth of the baryonic droplet by the increasing incompatibility from the cosmic expansion coincided with the growth of the baryonic droplet by gravitational instability from the cosmic expansion. The formation of galaxies is through both gravitational instability and the incompatibility between dark matter and baryonic matter. The pre-galactic universe consisted of the growing baryonic droplets surrounded by the dark matter halos, which connected among one another in the form of filaments and voids. These dark matter domains later became the dark matter halos, and the baryonic droplets became galaxies, clusters, and superclusters.

Incompatible materials separate from each other. The force to maintain the separation is the anti-expansion force to keep one material to expand into the region of other material. The dimensional incompatibility between the baryonic droplet and the dark matter halo is expressed as the interfacial zone between the two different matter domains as Fig. 8.

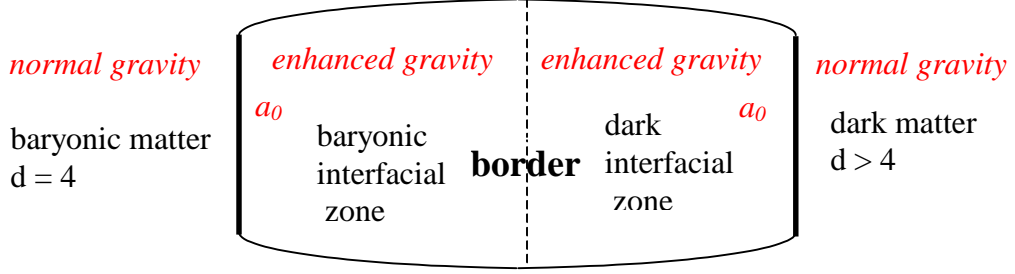


**Fig. 8:** the anti-expansion force in the interfacial zone between baryonic matter and dark matter. The region with the acceleration higher than  $a_0$  has normal gravity, and the interfacial zone with the acceleration lower than  $a_0$  has the enhanced gravity.

The baryon-dark border between baryonic matter and dark matter is in the middle of the interfacial zone. The interfacial zone consists of the dark interfacial zone and the baryonic matter zone for two sides of the baryon-dark border. The force in the interfacial zone is the anti-expansion force as the enhancement of gravity in the interfacial zone away from the baryon-dark border to maintain a clear border. Such enhancement of gravity is same as the enhancement of gravity in the M. Milgrom's [17] Modified Newtonian Dynamics (MOND).

The starting line of the interfacial zone has  $a_0$  as the acceleration. The Newtonian acceleration is  $a_N$ . In the interfacial zone,  $a_N < a_0$ . The effective acceleration  $a_b$  for the baryonic interfacial zone and the  $a_d$  for the dark interfacial zone are as follows.

$$\begin{aligned} a_b &= (a_N a_0)^{1/2} \\ a_d &= (a_N a_0)^{1/2} \end{aligned} \quad (9)$$

$$\text{enhancement of gravity away from the border} \propto (a_0 - a_N)^{1/2} \quad (10)$$

In the equilibrium state,  $a_b$  is symmetrical to  $a_d$ . At a distance,  $r$ , away from the border,

$$\begin{aligned} a_{b,r} &= a_{d,r} \\ (a_0 - a_N)_{b,r}^{1/2} &= (a_0 - a_N)_{d,r}^{1/2} \end{aligned} \quad (11)$$

The enhancement of gravity away from the border in the baryonic interfacial zone results in flat rotation curves as observed in some galaxies [18]. The enhancements of gravity away from the border in both interfacial zones are equal and cancel each other. The net anti-expansion force is zero. This cancellation of the enhancement of gravity is the global cancellation of the deviation (the anti-expansion force) between MOND and Newtonian gravity in a large area that is larger than the interfacial zones. The distance from the center of baryonic mass to the starting line of the interfacial zone increases with increasing  $a_0$ . The size of the universe is directly proportional to  $a_0$ .

As in emulsion, the size of the baryonic droplet grows with increasing incompatibility between dark matter and baryonic matter. As the incompatibility between dark matter and baryonic matter increases with increasing size of the universe, the droplet develops the droplet growth potential as the potential to increase the mass of the droplet. The droplet growth potential converts to the non-zero net anti-expansion force by moving the baryon-dark border outward to absorb free baryonic matter outside and to merge with other droplets. Such movement of the baryon-dark border is derived from the uneven enhancement of gravity in the interfacial zone: high enhancement of gravity away from the border in the dark interfacial zone and low or no enhancement of gravity away from the border in the baryonic interfacial zone.

$$\frac{a_{b,r}}{(a_0 - a_N)_{b,r}} < \frac{a_{d,r}}{(a_0 - a_N)_{d,r}} \quad (12)$$

In the extreme case,  $a_b = a_N$ , so there is low or no enhancement of gravity in the baryonic interfacial zone as observed as falling rotation curves in bright galaxies [18].

In the case of the trapping of free dark matter inside the baryonic droplet, the incompatibility between dark matter and baryonic matter generates the droplet contraction potential. The potential is to contract the droplet in order to remove the free dark matter inside. The droplet contraction potential converts to the non-zero net anti-expansion force by moving the baryon-dark border inward to expel free dark matter inside. The inward movement involves the uneven enhancement of gravity: low enhancement of gravity in the dark interfacial zone and high enhancement of gravity in the baryonic interfacial zone.

$$\frac{a_{b,r}}{(a_0 - a_N)_{b,r}} > \frac{a_{d,r}}{(a_0 - a_N)_{d,r}} \quad (13)$$

The high enhancement of gravity away from the border in the baryonic interfacial zone is observed as rising rotation curves in dwarfs and low surface brightness galaxies [18].

## 6. *The Evolution of Galaxies, Clusters, and Superclusters*

When there were many baryonic droplets, the merger among the baryonic droplets became another mechanism to increase the droplet size and mass. In Fig. 9, the baryonic droplets (A and B) merged into one droplet (C). When three or more droplets merged together, dark matter was likely trapped in the merged droplet (D, E, and F in Fig. 9). The droplet with trapped dark matter inside is the heterogeneous baryonic droplet, while the droplet without trapped dark matter inside is the homogeneous baryonic droplet.

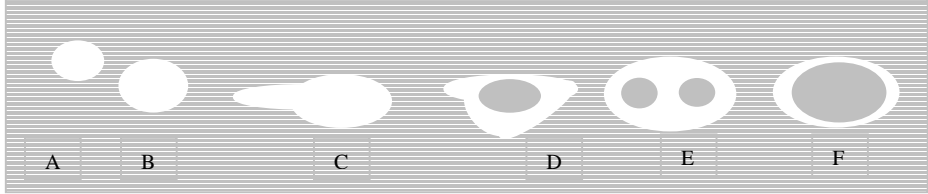


**Fig. 9:** the homogeneous baryonic droplets (A, B, and C), and the heterogeneous baryonic droplets (D, E, and F)

For the heterogeneous droplet, the dark matter core is essentially the dark droplet surrounded by the baryonic matter shell. As the dark droplet, the dark matter core has the droplet growth potential proportional to the size of the universe, and has the baryon-dark border moving toward the baryonic matter shell. Thus, two baryon-dark borders in the heterogeneous droplet are the external border between the dark matter halo and the and the dark matter halo and the internal baryon-dark border between the baryonic matter shell and the dark matter core. The external border moved toward the dark matter halo, while the internal border moved toward the baryonic matter shell. When a section of the internal border and a section of the external border merged, the dark matter from the dark matter core moved to the dark matter halo away from the heterogeneous droplet, and the droplet became homogeneous.

When the temperature dropped to  $\sim 1000^{\circ}\text{K}$ , some hydrogen atoms in the droplet paired up to create molecular baryonic matter. The most likely place to form such molecular baryonic matter was in the interior part of the droplet. For heterogeneous droplet, molecular baryonic matter formed a molecular layer around the core. Molecular hydrogen cooled the molecular layer by emitting infrared radiation after collision with atomic hydrogen. Eventually, the temperature of the molecular layer dropped to around 200 to  $300^{\circ}\text{K}$ , reducing the gas pressure and allowing the molecular layer to continue contracting into gravitationally bound dense molecular layer with high viscosity.

Without electromagnetism, the viscosity of dark matter remained low. The viscosity in the dense molecular layer around the core slowed the movement of the internal baryon-dark border toward the baryonic matter shell. On the other hand, the low-viscosity dark matter did not hinder the movement of the external baryon-dark border toward the dark matter halo. The increasing difference in the speeds of movement between the internal and external borders increased the fraction of the heterogeneous baryonic droplets.

Subsequently, the whole baryonic matter shell became the dense molecular layer. The dense baryonic matter shell contracted into gravitationally bound clumps, which prevented the movement of the internal border. The dark matter cores build up the internal pressure from the accumulated droplet growth potential. Eventually, the core with high internal pressure caused the eruption to the droplet. The dark matter rushed out of the droplet within a short time, and the baryonic matter shell collapsed. This eruption is much larger in area and much weaker in intensity than supernova. The “big eruption” of the baryonic droplet brings about the morphologies of galaxies.

If there was very small or no dark matter core as in the homogeneous baryonic droplet, the shape of the resulting galaxy is circular as in the  $E_0$  type elliptical galaxy. If the relative size of the dark matter core was small, the change in the shape of the shell was minor. It is like squeezing out orange juice (dark matter core) through one opening on the orange skin (baryonic matter shell). As the dark matter core moved out, the baryonic matter shell stretched in the opposite direction. The minor change resulted in an elliptical shape as in  $E_1$  to  $E_7$  elliptical galaxies, whose lengths of major axes are proportional to the relative sizes of the dark matter core.

During the collapse of the baryonic matter shell in the big eruption, the collision produced a shock front of high density, which resulted in the formation of many massive first stars. After few million years, such massive first stars became supernovas and black holes. Most of the massive first stars became black holes without contributing to the metal enrichment of the surrounding. The mergers of black holes generated the supermassive black hole as the nucleus of quasar. Such first quasar galaxies that occurred as early as  $z = 6.28$  were observed to have about the same sizes as the Milky Way [19].

The supernova shock wave induced the formation of stars in the exterior part of the droplet. The time difference in the formations of the nucleus and the formation of stars in the surface was not large, so there are small numbers of observed young stars in elliptical galaxies. This formation of galaxy follows the monolithic collapse model [20] in which baryonic gas in galaxies collapses to form stars within a very short period. Elliptical galaxies continue to grow slowly as the universe expands.

If the size of the dark matter core is medium (D in Fig. 9), it involves a large change on the baryonic matter shell. It is like to release air (the dark matter core) from a balloon (the baryonic matter shell) filled with air. As the dark matter core moved out, the baryonic matter shell moved in the opposite direction.

If there was only one opening as an air balloon with one opening, the dark matter stream from the dark matter core and the baryonic stream from the baryonic matter shell moved in opposite directions. Later, the two streams separated. The dark matter stream merges with the surrounding dark matter. The baryonic stream with high momentum penetrated the surrounding dark matter halo. As the baryonic stream penetrated into the dark matter halo, it met resistance from the anti-expansion force. Eventually, the stream stopped.

The minimization of the interfacial area due to the incomparability between baryonic matter and dark matter transformed the shape of the stream from linear to disk. (The minimization of the interfacial area is shown in the water bead formation on a wax paper.) To transform into disk shape, the stream underwent differential rotation with the increasing angular speeds toward the center. The fast angular speed around the center allowed the winding of the stream around the center. After few rotations, the structure consisted of a bungle was formed by wrapping the stream at the center and the attached spiral arms as spiral galaxy as Fig. 10.

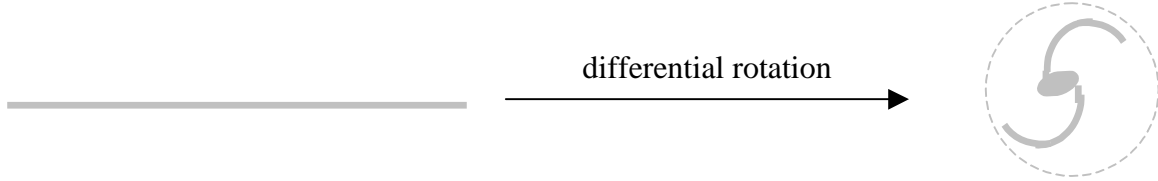


**Fig. 10:** from the linear baryonic stream to normal spiral galaxy with the baryon-dark border (dot line)

During the stream formation, the high-density region derived from the collision during the collapse spread out, so the density of the stream was too low to form stars. As the stream wrapped around at the center, the wrapping of the stream produces the high-density region for the star formation in a steady pace. Thus, the first stars and the black holes at the center in spiral galaxies are smaller than in elliptical galaxies. The stars at the center became black holes and supernovas that induced the star formation in spiral arms. The massive center area decreases the angular speed around the center, greatly retarding the winding of the spiral arms around the center. With this steady pace for the star formation, there are still many young stars in spiral galaxies. When there were more than one baryonic stream in the same general direction, there are more than two spiral arms.

Some streams went through the dark matter halos, and entered into the adjacent baryonic droplets. The adjacent droplet captured a part of the stream, and another part of the stream continued to move to the dark matter halo, and finally settled near the droplet in the dark matter halo. Dependent on the direction of the entry, the captured part of the stream later became a part of the disk of the host galaxy, star clusters in the halo, or both. The part of the stream that settled near the droplet became the dwarf spheroidal galaxy. Under continuous disruption and absorption of the tidal interaction from the large galaxy nearby, the dwarf spheroidal galaxy does not have well-defined baryonic-dark border, disk, and internal rotation.

When two connected dark matter cores inside far apart from each other (E in Fig. 9) generated two openings in opposite sides of the droplet, the momentum from the two opposite dark matter streams canceled each other nearly completely. The result was the slow moving baryonic droplet. Two opposite baryonic streams formed side by side with the two opposite dark matter streams. When the baryonic stream entered the dark matter halo, the size of the stream decreased due to the anti-expansion force by the dark matter, so there were the thick stream in the baryonic matter shell and the thin stream in the dark matter halo. As the baryonic stream penetrated into the dark matter halo, it met resistance from the anti-expansion force. Eventually, the stream stopped. The result after few differential rotations is the structure with one center, one bar from the thick stream stranding across the center, and arms attached to the bar as bar spiral galaxy as Fig. 11.

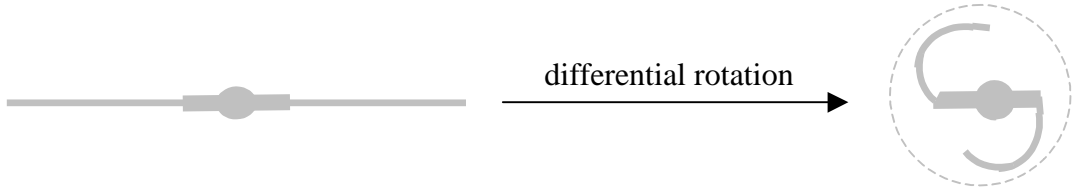


**Fig. 11:** from the barred linear baryonic stream to barred spiral galaxy with the baryon-dark border (dot line)

The result is barred spiral galaxy. As in normal spiral galaxy, the length of the spiral arm depends on the size of the dark matter core. The smallest dark matter core for barred spiral galaxy brings about SBa, and the largest dark matter core brings about SBd. The stars form in the low-density spiral arms much later than in the nucleus, so they are many young stars in the spiral arms.

If the size of the dark matter core was large (F in Fig. 9), the total dark matter mass was nearly large enough or large enough for dark matter to have low droplet growth potential. The escape of the dark matter from the droplet involved little or no eruption, resulting in the gradual migration of large amount of dark matter outward and the gradual migration of small amount of baryonic matter inward. Such opposite migrations are long and continuous processes. The result is irregular galaxy. When enough baryonic matter migrated to the center, and first star formation started. As baryonic matter continues migrating toward the center, the star formation continues in a slow rate up to the present time.

At the end of the big eruption, vast majority of baryonic matter was primordial free baryonic matter resided in dark matter outside of the galaxies from the big eruption. This free baryonic matter constituted the intergalactic medium (IGM). Stellar winds, supernova winds, and quasars provide heat and heavy elements to the IGM as ionized baryonic atoms. The heat prevented the formation of the baryonic droplet in the IGM.

Galaxies merged into new large galaxies, such as giant elliptical galaxy and cD galaxy ( $z > 1\text{-}2$ ). Similar to the transient molecular cloud formation from the ISM (interstellar medium) through turbulence, the tidal debris and turbulence from the mergers generated the numerous transient molecular regions, which located in a broad area [21]. The incompatibility between dark matter and baryonic matter transformed these transient molecular regions into the stable second-generation baryonic droplets surrounded by the dark matter halos. The baryonic droplets had much higher fraction of hydrogen molecules, much lower fraction of dark matter, higher density, and lower temperature, and lower entropy than the surrounding. The baryonic droplets started small with the enormous droplet growth potential. The rapid growth of the baryonic droplets drew large amount of the surrounding IGM inward, generating the IGM flow shown as the cooling flow. The IGM flow induced the galaxy flow. The IGM flow and the galaxy flow moved toward the merged galaxies, resulting in the protocluster ( $z \sim 0.5$ ) with the merged galaxies as the cluster center.

Before the protocluster stage, spirals grew normally and passively by absorbing gas from the IGM as the universe expanded. During the protocluster stage ( $z \sim 0.5$ ), the massive IGM flow injected a large amount of gas into the spirals that joined in the galaxy flow. Most of the injected hot gas passed through the spiral arms and settled in the bungle parts of the spirals. Such surges of gas absorption from the IGM flow resulted in major starbursts ( $z \sim 0.4$ ) [22]. Meanwhile, the nearby baryonic droplets continued to draw the IGM, and the IGM flow and the galaxy flow continued. The results were the formation of high-density region, where the galaxies and the baryonic droplets competed for the IGM as the gas reservoir. Eventually, the maturity of the baryonic droplets caused a decrease in drawing the IGM inward, resulting in the slow IGM flow. Subsequently, the depleted gas reservoir could not support the major starbursts ( $z \sim 0.3$ ). The galaxy harassment and the mergers in this high-density region disrupted the spiral arms of spirals, resulting in S0 galaxies with indistinct spiral arms ( $z \sim 0.1 - 0.25$ ). The transformation process of spirals into S0 galaxies started at the core first, and moved to the outside of the core. Thus, the fraction of spirals decreases with decreasing distance from the cluster center [22].

The static and slow-moving second-generation baryonic droplets turned into dwarf elliptical galaxies and globular clusters. The fast moving second-generation baryonic droplets formed the second-generation baryonic stream, which underwent a differential rotation to minimize the interfacial area between the dark matter and baryonic matter. The result is the formation of blue compact dwarf galaxies (BCD), such as NGC 2915 with very extended spiral arms. Since the star formation is steady and slow, so the stars formed in BCD are new.

The galaxies formed during  $z < 0.1-0.2$  are mostly metal-rich tidal dwarf galaxies (TDG) from tidal tails torn out from interacting galaxies. In some cases, the tidal tail and the baryonic droplet merge to generate the starbursts with higher fraction of molecule than the TDG formed by tidal tail alone [23].

When the interactions among large galaxies were mild, the mild turbulence caused the formation of few molecular regions, which located in narrow area close to the large galaxies [21]. Such few molecular regions resulted in few baryonic droplets, producing weak IGM flow and galaxy flow. The result is the formation of galaxy group, such as the Local Group, which has fewer dwarf galaxies and lower density environment than cluster.

Clusters merged to generate tidal debris and turbulence, producing the baryonic droplets, the ICM (intra-cluster medium) flow, and the cluster flow. The ICM flow and the cluster flow directed toward the merger areas among clusters and particularly the rich clusters with high numbers of galaxies. The ICM flow is shown as the warm filaments outside of cluster [24]. The dominant structural elements in superclusters are single or multi-branching filaments [25]. The cluster flow is shown by the tendency of the major axes of clusters to point toward neighboring clusters [26]. Eventually at the maximum incompatibility between dark matter and baryonic matter, the observable expanding universe will consist of giant voids and superclusters surrounded by the dark matter halos.

In summary, the whole observable expanding universe is the “Milky Universe” as one unit of emulsion with increasing incompatibility between dark matter and baryonic matter. The five periods of baryonic structure development are the free baryonic matter, the baryonic droplet, the galaxy, cluster, and the supercluster periods as Fig. 12. The first-

generation galaxies are elliptical, normal spiral, barred spiral, irregular, and dwarf spheroidal galaxies. The second-generation galaxies are giant ellipticals, cD, evolved S0, dwarf ellipticals, BCD, and TDG. The universe now is in the early part of the supercluster period.

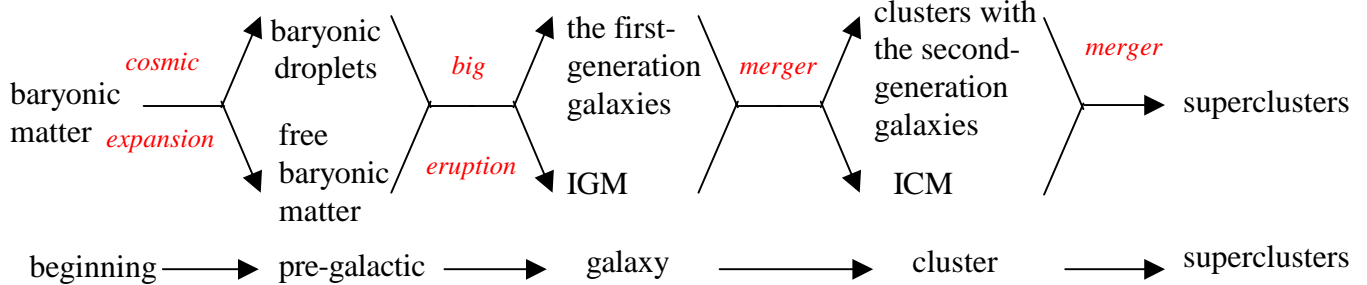


**Fig. 12:** the five levels of baryonic structure in the Milky Universe

## 7. *High-Energy Cosmic Rays*

Baryonic matter has four-dimensional space-time and four-mass dimensional mass, and dark matter has four-dimensional space-time and higher (from five to ten) mass dimensional masses. (Eleven-mass dimension is for gravity.) Derived from eq. (5), the masses of seven mass dimensional fermions from  $F_4$  to  $F_{10}$  are as follows.

$$M_{F_d} = M_{Planck} \alpha^{2(11-d)+1}, \quad (14)$$

where  $d = 4$  to  $10$ , and  $\alpha$  as the fine structure constant for electromagnetism is the same for all particles.

Dark matter has been detected only indirectly by means of its gravitational effects astronomically. Dark matter as weakly interacting massive particles (WIMPs) has not been detected directly on the earth [27]. This paper proposes that the absence of the direct detection of dark matter on the earth is due to the incompatibility between baryonic matter and dark matter, analogous to incompatible oil and water. The incompatibility means that when baryonic matter and dark matter are far away from each other, they attract each other through gravity, but when they are close together, they repel each other. The incompatibility leads to distribution of the dark matter and baryonic matter in different regions like emulsion. Most dark matter fermions form dark matter halos outside of baryonic galaxies. Some dark matter fermions remain inside of galaxies, such as the Milky Way Galaxy. The dark matter particles in the Milky Way Galaxy form the thin dark matter halos around star systems, such as the solar system. The repulsion in the thin dark matter halo causes Pioneer 10 and 11 space crafts in the outer space of the solar system to have anomalous acceleration toward the sun [28].

Over the range from  $10^9$  eV to over  $10^{20}$  eV, the “flux” of high-energy cosmic rays appears to follow a single power law  $E^{-\gamma}$ . The “energy spectrum” appears to be smooth

except few breaks. The power index,  $\gamma$ , increases from about 2.6 to 3 at  $E \sim 3 \times 10^{15}$  eV known as the “knee”, and decreases to 2.7 at  $E \sim 5 \times 10^{18}$  eV known as the “ankle”. The observed energy of the highest energy cosmic ray is  $\sim 3 \times 10^{20}$  eV [29].

Dark matter has been considered as the source of high-energy cosmic rays, particularly ultra high-energy cosmic rays [30]. This paper posits that high-energy cosmic rays come mainly from dark matter. The transformation from dark matter to baryonic cosmic ray starts from supernova. When dark matter particles are far away from baryon matter, dark matter particles exist as a single group in an equilibrium state without the distinct differentiation in mass dimensions. Supernova shocks accelerate dark matter particles to pass through turbulent baryonic interstellar medium (ISM). The diffusion of dark matter in turbulent ISM follows the Lagutin’s anomalous diffusion model [31] that describes the anomalous diffusion of the accelerated cosmic rays from supernova shocks in turbulent ISM. In the anomalous diffusion model, there are the subdiffusive regime and the superdiffusive regime. The diffusion of hybrid matter can be subdiffusive with the trapping as the extreme, or superdiffusive with the escape as the extreme. The anomalous diffusion model results in the power law energy spectrum for dark matter.

When dark matter passes through ISM, because of the incompatibility between dark matter and baryonic matter, the temporary trapping of dark matter transforms dark matter into “hybrid matter” that has characteristics of both dark matter and baryonic matter. In hybrid matter, the converted baryonic matter (basically hydrogen atom) is confined within hybrid matter with a definite energy, and its incompatibility with baryonic matter is much less than the dark matter’s incompatibility with baryonic matter. As the varying supersymmetry transformation mentioned above, the transformation of dark matter into hybrid matter is to fractionalize dark matter by eq. (5). Hybrid matter has its own energy spectrum in between the energy levels of various dark matter fermions, so instead of 11-d as in eq. (14), hybrid matter has  $(11-d)/2$ . The transformation starts from individual dark matter fermion,  $F_d$ , rather than from Planck particle as in eq. (14). To have hydrogen atom as the confined baryonic matter, hybrid matter is boson instead of fermion, so it is  $2n-1$  as eq. (4b) to transform dark matter fermion into hybrid matter boson. Therefore, derived from eq. (5) and eq. (14), the equation for the hybrid matter energy spectrum from the transformation of dark matter fermion,  $F_d$ , is shown in eq. (15).

$$E_{H, d, n} \geq E_{0, d} \alpha^{\frac{(11-d)(2n-1)}{2}}, \quad (15)$$

where  $E_{H, d, n}$  = hybrid matter boson energy from dark matter fermion,  $F_d$ , with  $d$  mass dimension and with the  $n$  order of hybrid matter,  $E_{0, d}$  = the rest energy of  $F_d$ , and  $\alpha$  = fine structure constant of electromagnetism. The first transformation process produces the “first order hybrid matter boson” with  $n = 1$  from  $F_d$ . There are more orders of hybrid matter from  $F_d$  until the resulting energy for the hybrid matter from the transformation process is equal to or below the rest energy of  $F_{d-1}$ . The minimum energy for  $E_{H, d, n}$  is the rest energy, and the additional energy comes from kinetic energy.

From eq. (14),  $E_{0, d}$ ’s are  $1.3 \times 10^{13}$  eV,  $2.5 \times 10^{17}$  eV, and  $4.7 \times 10^{21}$  eV for  $F_8$ ,  $F_9$ , and  $F_{10}$ , respectively, which relate to hybrid matter. The calculation by eq. (15) shows that

there are only four possible hybrid matter bosons:  $E_{H,8,1} \geq 8 \times 10^9$  eV,  $E_{H,9,1} \geq 2 \times 10^{15}$  eV,  $E_{H,10,2} \geq 2 \times 10^{18}$  eV, and  $E_{H,10,1} \geq 4 \times 10^{20}$  eV. The energies of the first order hybrid matters for dark matter fermions below  $F_8$  are equal to or below the rest energy of  $F_{d-1}$ . Thus, there is no hybrid matter from  $F_7$ ,  $F_6$ , and  $F_5$ .

When hybrid matter collides with the earth, which is the permanent trap, unlike the temporary trap as in ISM, the hybrid matter converts into baryonic matter permanently as high-energy cosmic rays. The calculated values of  $E_{H,8,1}$ ,  $E_{H,9,1}$ ,  $E_{H,10,2}$ , and  $E_{H,10,1}$  are in good agreement with the observed values for the low-energy cutoff, the knee, the ankle, and the high-energy cutoff, respectively, of high-energy cosmic ray.

In summary, the periodic table of elementary particles is expanded to include dark matter fermions and hybrid matter bosons that become high-energy cosmic rays. The transformation of few dark matter particles inside galaxies to baryonic matter is the source of high-energy cosmic rays. The transformation process involves four hybrid matter bosons, representing respectively, the low-energy cutoff, the knee, the ankle, and the high-energy cutoff of high-energy cosmic rays. The calculated values (eq. (14) and eq. (15)) for the low-energy cutoff, the knee, the ankle, and the high-energy cutoff are in agreement with the observed values.

### Part 3: The Periodic Table of Elementary Particles

#### 8. *The Force Fields: the Masses of Gauge Bosons*

The third major part of the cosmic evolution is the periodic table of elementary particles for our baryonic matter. This part also includes the composition of hadrons and high-energy cosmic rays. The part deals with the three sets of seven orbitals (principal, auxiliary, and hadronic) that explain all elementary particles and hadrons.

During the simultaneous fission, the mixed particles with the CP symmetry between internal brane and antibrane result in annihilation to become cosmic radiation. The particles that are not annihilated have asymmetrical charge-parity (CP asymmetry), in such way that the mixed particle has two asymmetrical sets of seven dimensional orbitals. The two sets of dimensional orbitals are “principal dimensional orbital” and “auxiliary dimensional orbital”. The auxiliary set is dependent on the principal set, so the mixed particle appears to have only one set of dimensional orbital. Auxiliary dimensional orbital is the hidden dimensional orbital.

For the four-mass-dimensional particle (baryonic matter), the two sets of seven dimensional orbitals are principal dimensional orbital and auxiliary dimensional orbital. These hierarchical dimensional orbitals are the force and mass fields, including gravity, as shown in Fig. 13.

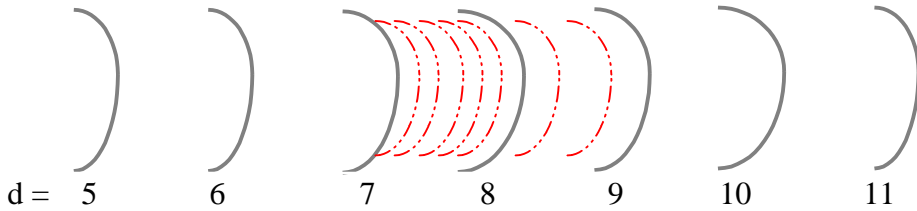


**Fig. 13:** dimensional orbitals in the four-mass dimensional (4d) particle (baryonic matter): principal dimensional orbital (solid line), and auxiliary dimensional orbital (dot line),  $d$  = principal dimensional orbital number

As shown in Fig. 13, the seven orbitals of hidden auxiliary dimensional orbital are in the middle of the seven orbitals of principal dimensional orbital.

The structure of the 4d particle with dimensional orbitals resembles to the structure of atomic orbital. Consequently, the periodic table of elementary particles is constructed to account of all leptons, quarks, gauge bosons, and hadrons.

For the gauge bosons, the seven orbitals of principal dimensional orbital are arranged as  $F_5 B_5 F_6 B_6 F_7 B_7 F_8 B_8 F_9 B_9 F_{10} B_{10} F_{11} B_{11}$ , where  $B$  and  $F$  are boson and fermion in each orbital. The mass dimension in Eq. (5) becomes the orbitals in principal dimensional orbital with the same equations.

$$M_{d,F} = M_{d,B} \alpha_{d,B} \quad (16a)$$

$$M_{d-1,B} = M_{d,F} \alpha_{d,F}, \quad (16b)$$

$$M_{d-1,B} = M_{d,B} \alpha_d^2, \quad (16c)$$

where  $D$  is the principal dimensional orbital number from 6 to 11.  $E_{5,B}$  and  $E_{11,B}$  are the energies for the 5d principal dimensional orbital and the 11d principal dimensional orbital, respectively. The lowest energy is the Coulombic field,

$$E_{5,B} = \alpha E_{6,F} = \alpha M_e \quad (17)$$

The bosons generated are the principal dimensional orbital bosons or  $B_D$ . Using only  $\alpha_e$ , the mass of electron ( $M_e$ ), the mass of  $Z^0$ , and the number (seven) of dimensional orbitals, the masses of  $B_D$  as the gauge boson can be calculated as shown in Table 1.

**Table 1.** The Masses of the principal dimensional orbital bosons: $\alpha = \alpha_e$ ,  $d = \text{principal dimensional orbital number}$ 

$B_d$	$M_d$	GeV (calculated)	Gauge boson	Interaction, symmetry	Predecessor
$B_5$	$M_e \alpha$	$3.7 \times 10^{-6}$	A	Electromagnetic, $U(1)$	pre-charged
$B_6$	$M_e/\alpha$	$7 \times 10^{-2}$	$\pi_{1/2}$	Strong, $SU(3) \rightarrow U(1)$	pre-strong
$B_7$	$M_6/\alpha_w^2 \cos \theta_w$	91.177 (given)	$Z_L^0$	weak (left), $SU(2)_L$	Fractionalization
$B_8$	$M_7/\alpha^2$	$1.7 \times 10^6$	$X_R$	CP (right) nonconservation, $U(1)_R$ CP asymmetry	
$B_9$	$M_8/\alpha^2$	$3.2 \times 10^{10}$	$X_L$	CP (left) nonconservation, $U(1)_L$ CP asymmetry	
$B_{10}$	$M_9/\alpha^2$	$6.0 \times 10^{14}$	$Z_R^0$	weak (right), $SU(2)_R$	Fractionalization
$B_{11}$	$M_{10}/\alpha^2$	$1.1 \times 10^{19}$	G	gravity, D particle in D+1 bulk	Pregravity

In Table 1,  $\alpha = \alpha_e$  (the fine structure constant for electromagnetic field), and  $\alpha_w$  is not same as  $\alpha$  of the rest, because as shown later, there is a mixing between  $B_5$  and  $B_7$  as the symmetry mixing between  $U(1)$  and  $SU(2)$  in the standard theory of the electroweak interaction, and  $\sin \theta_w$  is not equal to 1. As shown later,  $B_5$ ,  $B_6$ ,  $B_7$ ,  $B_8$ ,  $B_9$ , and  $B_{10}$  are A (massless photon),  $\pi_{1/2}$ ,  $Z_L^0$ ,  $X_R$ ,  $X_L$ , and  $Z_R^0$ , respectively, responsible for the electromagnetic field, the strong interaction, the weak (left handed) interaction, the CP (right handed) nonconservation, the CP (left handed) nonconservation, and the P (right handed) nonconservation, respectively. The calculated value for  $\theta_w$  is  $29.69^\circ$  in good agreement with  $28.7^\circ$  for the observed value of  $\theta_w$  [32]. The calculated energy for  $B_{11}$  is  $1.1 \times 10^{19}$  GeV in good agreement with the Planck mass,  $1.2 \times 10^{19}$  GeV.

There are dualities between dimensional orbitals and the cosmic evolution. The pre-charged force, the pre-strong force, the fractionalization during the superluminal inflation, the CP asymmetry to generate matter during the fission, and the pregravity are the predecessors of electromagnetic force, the strong force, the weak interaction, the CP nonconservation, and gravity, respectively. These forces are manifested in the principal dimensional orbitals with various space-time symmetries and gauge symmetries. The strengths of these forces are different than their predecessors, and are arranged according to the dimensional orbitals. Each of the forces will be discussed as follows.

The pre-charged force is the predecessor of electromagnetism as the long-ranged force with the absorption-emission of massless particles with  $U(1)$  symmetry. Being the principal dimensional orbital with the lowest mass,  $B_5$  is the utmost orbital, so as the utmost pre-charged force in the 10D X 1D Kaluza-Klein structure, electromagnetism is  $B_5$ .

There is duality between the collapse of the pre-expanding universe and electromagnetism. The attraction between the 9-brane and the 9-antibrane is manifested as electric force. As the collapse of the pre-expanding universe begins, and the 9-brane and the 9-antibrane start to move, the attractive force and the repulsive force cause an inversion that turns the 9-brane and the 9-antibrane inside, and turns pregravity and the anti-pregravity outside. In the observable universe, there is no repulsive force between pregravity and the anti-pregravity, so the force for the inversion is manifested as the force

for the rotation, which is magnetic force, perpendicular to the direction of moving charging particles.

Only the 4d particle (baryonic matter) has the  $B_5$ , so without  $B_5$ , dark matter consists of permanently neutral higher dimensional particles. It cannot emit light, cannot form atoms, and exists as neutral gas.

The short-ranged pre-strong force is the predecessor of the short-ranged strong force for quarks with the absorption-emission of massless particles through non-zero energy medium, pions. The pre-strong force is next to the pre-charged force, so the strong force for quarks is  $B_6$  next to  $B_5$  for electromagnetism. There is duality between  $B_6$  and the hiding of quark as the auxiliary particle in the 4d particle. Lepton is the principal particle.

The hypercharges for both  $e^+$  and  $\nu$  are 1, while for both  $u$  and  $d$  quarks, they are 1/3. The electric charges for  $e^+$  and  $\nu$  are 1 and 0, respectively, while for  $u$  and  $d$  quarks, they are 2/3 and -1/3, respectively. The hiding of quark is achieved by the strong interaction for quark. The gauge boson is  $B_6$ , whose mass is one half of pion. Section 11 will deals with the strong interaction.

The fractionalization of the particles during the inflation is the predecessor of the weak interaction for the changes of the flavors (masses) of particles. The two fractionalizations in the opposite sides (hidden and observable) of the expanding universe are chiral, so the weak interaction is chiral. The fractionalization involves the uneven supersymmetry transformation of a particle into a lower dimensional and lower mass particle. In the weak interaction, gauge symmetry for the absorption and the emission of massive particle replaces the supersymmetry transformation that is no longer possible. The method for such replacement is for the weak interaction to take part in the formation of electric charge, which involves the absorption and the emission of massless particle. It is the  $U(1) \times SU(2)$  mixing to form electric charge.  $U(1)$  is the non-fractionalization from the pre-electromagnetism, so assign hypercharge of 1 to both pre- $e^+$  and pre- $\nu$ , respectively. In  $SU(2)$ , pre- $e^+$  and pre- $\nu$  are before and after the fractionalization, respectively, so assign isospin 1/2 and -1/2 to pre- $e^+$  and pre- $\nu$ , respectively. The mixing of  $U(1)$  and  $SU(2)$  leads to electric charge = hypercharge/2 + isospin. The electric charges of  $e^+$  and  $\nu$  are equal to 1 and 0, respectively.

$B_7$  carries the charge for the gauge symmetry for the weak interaction within the family of leptons or quarks at different dimensional orbitals. There is the mixing between  $B_5$  and  $B_7$ , corresponding to the  $U(1) \times SU(2)$  mixing. The absolute or nearly absolute chiral symmetry (permanent chirality) generates massless or nearly massless neutrinos.

The CP asymmetry to generate matter during the fission is the predecessor of the CP nonconservation that is  $B_9$  for CP (left) with  $U(1)$  symmetry. For the reason of symmetry, P and CP nonconservations are in pairs of the right and the left.  $B_7$ ,  $B_8$ ,  $B_9$ , and  $B_{10}$  carry P (left), CP (right), CP (left), and P (right) nonconservation, respectively. However, only P (left) at  $B_7$  and CP (left) at  $B_9$  relate to the fractionalization and the CP asymmetry to generate matter, respectively, in the observable universe.

The principal dimensional boson,  $B_8$ , is a CP (right). The ratio of the force constants between the CP-invariant  $W_L$  in  $B_8$  and the CP-violating  $X_R$  in  $B_8$  is

$$\begin{aligned}\frac{G_8}{G_7} &= \frac{\alpha E_7^2 \cos^2 \Theta_W}{\alpha_W E_8^2} \\ &= 5.3 \times 10^{-10} ,\end{aligned}\tag{18}$$

which is in the same order as the ratio of the force constants between the CP-invariant weak interaction and the CP-violating interaction with  $|\Delta S| = 2$ . The  $B_8$  does not generate matter.

The principal dimensional boson,  $B_9 (X_L)$ , has the CP-violating  $U(1)_L$  symmetry.  $B_9$  generates matter. The ratio of force constants between  $X_R$  with CP conservation and  $X_L$  with CP-nonconservation is

$$\begin{aligned}\frac{G_9}{G_8} &= \frac{\alpha E_8^2}{\alpha E_9^2} \\ &= 2.8 \times 10^{-9} ,\end{aligned}\tag{21}$$

which is the ratio of the numbers between matter (dark and baryonic) and photons in the universe. During the simultaneous fission into dark matter and baryonic matter, the number of baryonic matter particles is 1/6 of total matter particles. Hence, the ratio of the numbers between baryonic matter and photons is about  $4.7 \times 10^{-10}$ , which is close to the ratio (around  $5 \times 10^{-10}$ ) obtained by the big bang nucleosynthesis.

Gravity, the individualized pregravity, continues to have the same long-ranged force with the Planck-infinite dimension as pregravity. Therefore, gravity continues to be  $B_{11}$  with the Planck mass. The summary of all forces and their predecessors is in Table 1.

## 9. *The Periodic Table of Elementary Particles: the Masses of Leptons and Quarks*

The two sets of seven dimensional orbitals result in 14 dimensional orbitals (Fig. 14) for gauge bosons, leptons, and quarks. The periodic table for elementary particles is shown in Table 2.

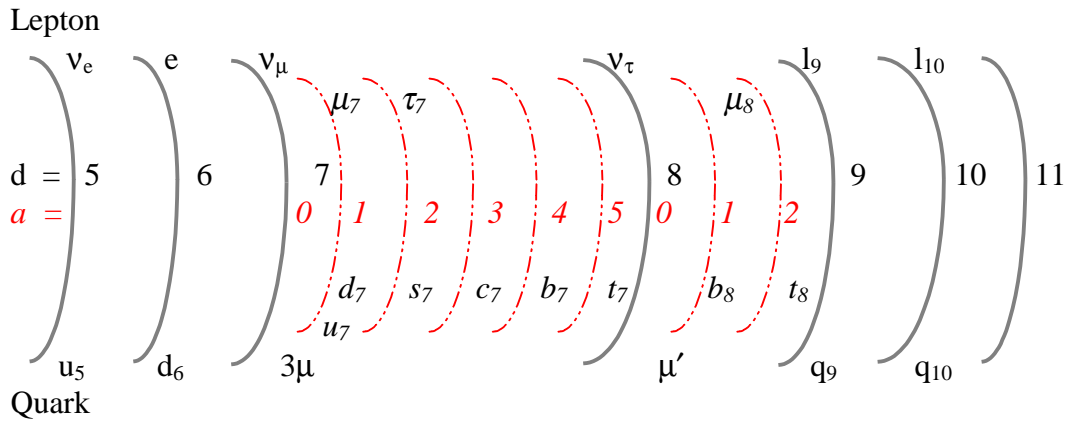


**Fig. 14:** leptons and quarks in the principal and auxiliary dimensional orbitals    d = principal dimensional orbital (solid line) number, a = auxiliary dimensional orbital (dot line) number

**Table 2.** The Periodic Table of elementary particles

d = principal dimensional orbital number, a = auxiliary dimensional orbital number

d	a = 0	1	2	a = 0	1	2	3	4	5
	<u>Lepton</u>			<u>Quark</u>			<u>Boson</u>		
5	$l_5 = \nu_e$			$q_5 = u_5 = 3\nu_e$			$B_5 = A$		
6	$l_6 = e$			$q_6 = d_6 = 3e$			$B_6 = \pi_{1/2}$		
7	$l_7 = \nu_\mu$	$\mu_7$	$\tau_7$	$q_7 = 3\mu$	$u_7/d_7$	$s_7$	$c_7$	$b_7$	$t_7$
8	$l_8 = \nu_\tau$	$\mu_8$		$q_8 = \mu'$	$b_8$	$t_8$			$B_8 = X_R$
9	$l_9$			$q_9$					$B_9 = X_L$
10	$f_{10}$								$B_{10} = Z_R^0$
11	$f_{11}$								$B_{11} = G$

“d” is the principal dimensional orbital number, and a is the auxiliary dimensional orbital number. (Note that  $F_d$  has lower energy than  $B_d$ .)

There are two types of fermions in the periodic table of elementary particles: low-mass leptons and high-mass leptons and quarks. Low-mass leptons include  $\nu_e$ ,  $e$ ,  $\nu_\mu$ , and  $\nu_\tau$ , which are in principal dimensional orbital, not in auxiliary dimensional orbital.  $l_d$  is denoted as lepton with principal dimension number, d.  $l_5$ ,  $l_6$ ,  $l_7$ , and  $l_8$  are  $\nu_e$ ,  $e$ ,  $\nu_\mu$ , and  $\nu_\tau$ , respectively. All neutrinos have zero mass because of chiral symmetry (permanent chiral symmetry).

High-mass leptons and quarks include  $\mu$ ,  $\tau$ ,  $u$ ,  $d$ ,  $s$ ,  $c$ ,  $b$ , and  $t$ , which are the combinations of both principal dimensional fermions and auxiliary dimensional fermions. Each fermion can be defined by principal dimensional orbital numbers (d's) and auxiliary dimensional orbital numbers (a's) as  $d_a$  in Table 3. For examples,  $e$  is  $6_0$  that means it has d

(principal dimensional orbital number) = 6 and a (auxiliary dimensional orbital number) = 0, so  $e$  is a principal dimensional fermion.

High-mass leptons,  $\mu$  and  $\tau$ , are the combinations of principal dimensional fermions,  $e$  and  $\nu_\mu$ , and auxiliary dimensional fermions. For example,  $\mu$  is the combination of  $e$ ,  $\nu_\mu$ , and  $\mu_7$ , which is  $7_1$  that has  $d = 7$  and  $a = 1$ .

Quarks are the combinations of principal dimensional quarks ( $q_d$ ) and auxiliary dimensional quarks. The principal dimensional fermion for quark is derived from principal dimensional lepton. To generate a principal dimensional quark in principal dimensional orbital from a lepton in the same principal dimensional orbital is to add the lepton to the boson from the combined lepton-antilepton. Thus, the mass of the quark is three times of the mass of the corresponding lepton in the same dimension. The equation for the mass of principal dimensional fermion for quark is

$$M_{q_d} = 3M_{l_d} \quad (20)$$

For principal dimensional quarks,  $q_5$  ( $5_0$ ) and  $q_6$  ( $6_0$ ) are  $3\nu_e$  and  $3e$ , respectively. Since  $l_7$  is massless  $\nu_\mu$ ,  $\nu_\mu$  is replaced by  $\mu$ , and  $q_7$  is  $3\mu$ . Quarks are the combinations of principal dimensional quarks,  $q_d$ , and auxiliary dimensional quarks. For example,  $s$  quark is the combination of  $q_6$  ( $3e$ ),  $q_7$  ( $3\mu$ ) and  $s_7$  (auxiliary dimensional quark =  $7_2$ ).

Each fermion can be defined by principal dimensional orbital numbers (d's) and auxiliary dimensional orbital numbers (a's). All leptons and quarks with d's, a's and the calculated masses are listed in Table 3.

**Table 3.** The Compositions and the Constituent Masses of Leptons and Quarks  
d = principal dimensional orbital number and a = auxiliary dimensional orbital number

	da	Composition	Calculated Mass
<u>Leptons</u>	<u>da for leptons</u>		
$\nu_e$	$5_0$	$\nu_e$	0
$e$	$6_0$	$e$	0.51 MeV (given)
$\nu_\mu$	$7_0$	$\nu_\mu$	0
$\nu_\tau$	$8_0$	$\nu_\tau$	0
$\mu$	$6_0 + 7_0 + 7_1$	$e + \nu_\mu + \mu_7$	105.6 MeV
$\tau$	$6_0 + 7_0 + 7_2$	$e + \nu_\mu + \tau_7$	1786 MeV
$\mu'$	$6_0 + 7_0 + 7_2 + 8_0 + 8_1$	$e + \nu_\mu + \mu_7 + \nu_\tau + \mu_8$	136.9 GeV
<u>Quarks</u>	<u>da for quarks</u>		
$u$	$5_0 + 7_0 + 7_1$	$q_5 + q_7 + u_7$	330.8 MeV
$d$	$6_0 + 7_0 + 7_1$	$q_6 + q_7 + d_7$	332.3 MeV
$s$	$6_0 + 7_0 + 7_2$	$q_6 + q_7 + s_7$	558 MeV
$c$	$5_0 + 7_0 + 7_3$	$q_5 + q_7 + c_7$	1701 MeV
$b$	$6_0 + 7_0 + 7_4$	$q_6 + q_7 + b_7$	5318 MeV
$t$	$5_0 + 7_0 + 7_5 + 8_0 + 8_2$	$q_5 + q_7 + t_7 + q_8 + t_8$	176.5 GeV

The principal dimensional fermion for heavy leptons ( $\mu$  and  $\tau$ ) is  $e$  and  $\nu_e$ . Auxiliary dimensional fermion is derived from principal dimensional boson in the same way as Eq. (5) to relate the energies for fermion and boson. For the mass of auxiliary dimensional fermion (AF) from principal dimensional boson (B), the equation is Eq. (21).

$$M_{AF_{d,a}} = \frac{M_{B_{d-1,0}}}{\alpha_a} \sum_{a=0}^a a^4 \quad , \quad (21)$$

where  $\alpha_a$  = auxiliary dimensional fine structure constant, and  $a$  = auxiliary dimension number = 0 or integer. The first term,  $\frac{M_{B_{d-1,0}}}{\alpha_a}$ , of the mass formula (Eq.(21)) for the auxiliary dimensional fermions is derived from the mass equation, Eq. (5), for the principal dimensional fermions and bosons. The second term,  $\sum_{a=0}^a a^4$ , of the mass formula is for Bohr-Sommerfeld quantization for a charge - dipole interaction in a circular orbit as described by A. Barut [1]. As in Barut lepton mass formula,  $1/\alpha_a$  is 3/2. The coefficient, 3/2, is to convert the principal dimensional boson mass to the mass of the auxiliary dimensional fermion in the higher dimension by adding the boson mass to its fermion mass which is one-half of the boson mass. Using Eq. (5), Eq. (21) becomes the formula for the mass of auxiliary dimensional fermions (AF).

$$\begin{aligned} M_{AF_{d,a}} &= \frac{3M_{B_{d-1,0}}}{2} \sum_{a=0}^a a^4 \\ &= \frac{3M_{F_{d-1,0}}}{2\alpha_{d-1}} \sum_{a=0}^a a^4 \\ &= \frac{3}{2} M_{F_{d,0}} \alpha_d \sum_{a=0}^a a^4 \end{aligned} \quad (22)$$

The mass of this auxiliary dimensional fermion is added to the sum of masses from the corresponding principal dimensional fermions (F's) with the same electric charge or the same dimension. The corresponding principal dimensional leptons for  $u$  (2/3 charge) and  $d$  (-1/3 charge) are  $\nu_e$  (0 charge) and  $e$  (-1 charge), respectively, by adding -2/3 charge to the charges of  $u$  and  $d$  [33]. The fermion mass formula for heavy leptons is derived as follows.

$$\begin{aligned}
M_{F_{d,a}} &= \sum M_F + M_{AF_{d,a}} \\
&= \sum M_F + \frac{3M_{B_{d-1,0}}}{2} \sum_{a=0}^a a^4
\end{aligned} \tag{23a}$$

$$= \sum M_F + \frac{3M_{F_{d-1,0}}}{2\alpha_{d-1}} \sum_{a=0}^a a^4 \tag{23b}$$

$$= \sum M_F + \frac{3}{2} M_{F_{d,0}} \alpha_d \sum_{a=0}^a a^4 \tag{23c}$$

Eq. (23b) is for the calculations of the masses of leptons. The principal dimensional fermion in the first term is  $e$ . Eq. (23b) can be rewritten as Eq. (24).

$$M_a = M_e + \frac{3M_e}{2\alpha} \sum_{a=0}^a a^4, \tag{24}$$

$a = 0, 1$ , and  $2$  are for  $e, \mu$ , and  $\tau$ , respectively. It is identical to the Barut lepton mass formula.

The auxiliary dimensional quarks except a part of  $t$  quark are  $q_7$ 's. Eq.(23c) is used to calculate the masses of quarks. The principal dimensional quarks include  $3v_\mu, 3e$ , and  $3\mu$ ,  $\alpha_7 = \alpha_w$ , and  $q_7 = 3\mu$ . Eq. (23c) can be rewritten as the quark mass formula.

$$M_q = \sum M_F + \frac{3\alpha_w M_{3\mu}}{2} \sum_{a=0}^a a^4, \tag{25}$$

where  $a = 1, 2, 3, 4$ , and  $5$  for  $u/d, s, c, b$ , and a part of  $t$ , respectively.

To match  $l_8 (v_\tau)$ , quarks include  $q_8$  as a part of  $t$  quark. In the same way that  $q_7 = 3\mu$ ,  $q_8$  involves  $\mu'$ .  $\mu'$  is the sum of  $e, \mu$ , and  $\mu_8$  (auxiliary dimensional lepton). Using Eq. (23a), the mass of  $\mu_8$  is equal to  $3/2$  of the mass of  $B_7$ , which is  $Z^0$ . Because there are only three families for leptons,  $\mu'$  is the extra lepton, which is "hidden".  $\mu'$  can appear only as  $\mu +$  photon. The pairing of  $\mu + \mu$  from the hidden  $\mu'$  and regular  $\mu$  may account for the occurrence of same sign dilepton in the high energy level [33]. The principal dimensional quark of  $t$  quark is  $\mu'$  instead of  $3\mu'$ , because  $\mu'$  is hidden, and  $t$  quark does not need to be  $3\mu'$  to be different. Using the equation similar to Eq.(25), the calculation for  $t$  quark involves  $\alpha_8 = \alpha, \mu'$  instead of  $3\mu$  for principal fermion, and  $a = 1$  and  $2$  for  $b_8$  and  $t_8$ , respectively. The hiding of  $\mu'$  for leptons is balanced by the hiding of  $b_8$  for quarks.

The calculated masses are in good agreement with the observed constituent masses of leptons and quarks [34][35]. The mass of the top quark in Reference [35] is  $174.3 \pm 5.1$  GeV

in a good agreement with the calculated value, 176.5 GeV. The masses of leptons, quarks, gauge bosons, and hadrons are calculated with only four known constants: the number of spatial dimensions, the mass of electron, the mass of  $Z^0$ , and  $\alpha_e$ .

## 10. *The Composition of Hadrons*

Auxiliary dimensional orbital is dependent on principal dimensional orbital, so quarks from auxiliary dimensional orbital cannot have independent existences with fractional electric charges and hypercharges. Quarks can exist only as the composites that have integral charges and hypercharges. Thus, another set of dimensional orbitals is required for such composites of quarks. This set of dimensional orbital is hadronic dimensional orbital that also has seven orbitals as in principal dimensional orbital and auxiliary dimensional orbital. Hadronic dimensional orbital is the third set of the three sets of seven orbitals.

Hadronic dimensional orbital is found by P. Polazzi [3]. Polazzi explains the relation between lifetimes and masses in terms of the shell structure in atomic orbital. The noble gases (stable atoms), He, Ne, Ar, Kr, Xe, and Rn have the shell numbers, 1, 2, 3, 4, 5, and 6, respectively. The cube root of the number of electrons for noble gases as a function of the shell numbers is a straight line. He finds that the cube root of the masses for stable hadrons as the function of order of these stable hadrons is a straight line. The stable atoms can be explained by atomic orbital, so the stable hadrons can be explained by the hadronic dimensional orbital.

The ground state of hadronic dimensional orbital starts from  $d = 6$ , which is  $\pi_{1/2}$ , the pseudoscalar quark. For hadronic dimensional orbital, the composite of quarks is  $2\pi_{1/2}$ . The hadronic dimensional orbital number ( $h$ ) is 0 for  $2\pi_{1/2}$ . The highest orbital ( $h = 7$ ) is the seventh orbital consisting of the combination of two highest mesonic quarks (b's). For baryon, it is after  $d = 7$ , and starts from  $h = 2$ . For baryon, the hadron at  $h = 2$  is proton. Fig. 2 shows the hadronic dimensional orbital with the hadronic number,  $h$ , and the mesons and the baryons representing the hadronic dimensional orbitals.

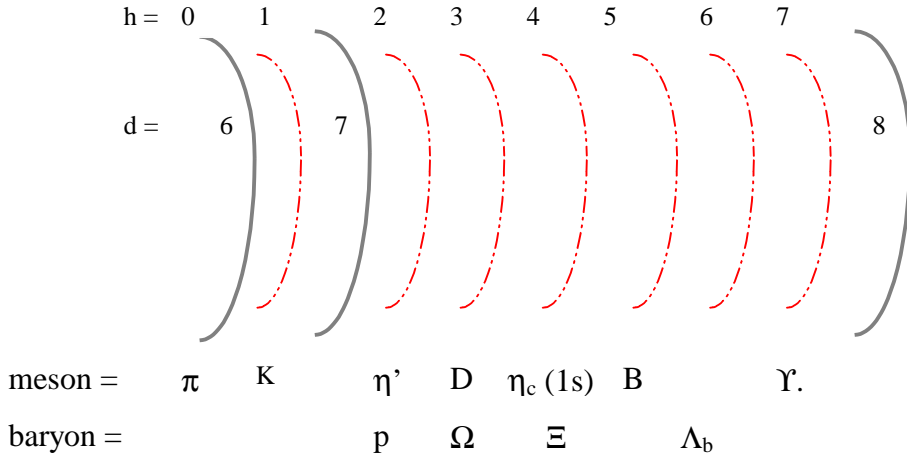


**Fig. 15:** Hadronic dimensional orbital, d = principal dimensional orbital (solid line) number, h = hadronic dimensional orbital (dot line) number

The entity in each orbital is denoted as “hadronic mark”. Instead of the fourth power of the auxiliary dimensional orbital number as in the quark mass formula, the mass in the hadronic mark mass formula is the third power of the hadronic number as in atomic orbital.

$$M_h = M_0 \sum_{h=0}^h (1+k h)^3, \quad (26)$$

where  $M_h$  = the mass of hadronic mark with  $h$  hadronic number,  $M_0$  is the ground state mass for hadronic mark,  $h$  = hadronic number, and  $k$  = constant.

Hadronic mark can be mesonic mark (MB) or baryonic mark (BM). For mesons, to connect exactly 140.05 MeV (two  $\pi_{1/2}$ 's) at  $h = 0$  and 10635.4 MeV (two b quarks) at  $h = 7$ ,  $M_0 = 140.05$  MeV and  $k = 0.268357$ . The masses for MM0, MM1, MM2, MM3, MM4, MM5, MM6, and MM7 are 140.05 (two  $\pi_{1/2}$ 's), 425.8, 934, 1758, 3006, 4805, 7295, and 10635 (two b quarks) MeV, respectively. The stable baryons start at  $h = 2$  with proton,  $p$  with the mass of 938.27 MeV near MM2 (934MeV). For baryons, the exact mass for BM4 is 2589.8 MeV as the combined mass for u, s, and c quarks. For baryons, to connect exactly 938.27 MeV ( $p$ ) for BM2 and 2589.8 MeV (u, s, and c quarks) for BM4,  $M_0 = 176.098$  MeV and  $k = 0.19095$ . The masses for BM0, BM1, BM2, BM3, BM4, BM5, BM6, and BM7 are 176.1, 473.6, 938.3 ( $p$ ), 1624, 2590 (usc), 3905, 5645, and 7891 MeV. The hadronic marks represent the stable hadrons, the significant parts of stable hadrons, and recurrent parts of all hadrons. As shown later, for mesons, MM0, MM1, MM2, MM3, MM4, MM5, and MM7  $\pi$ ,  $K$ ,  $\eta'$ ,  $D$ ,  $J/\Psi$  and  $\eta_c$  (1s),  $B$ , and  $\Upsilon$ , respectively. For baryons, BM2, BM3, BM4, and BM6 represent  $p$ ,  $\Omega$ ,  $\Xi$ , and  $\Lambda_b$ , respectively. The 1/3 power of mass as the function of the hadronic number is a straight line as shown in Fig. 16.

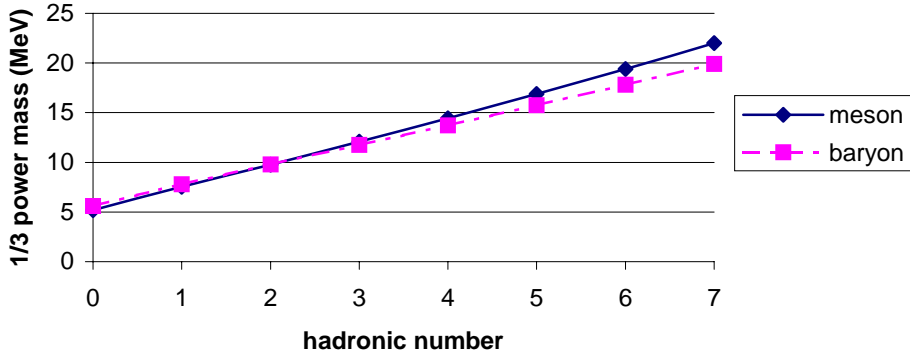


**Fig. 16:** Hadronic dimensional numbers and 1/3 power of hadron masses

Quarks from auxiliary dimensional orbital and hadronic marks from hadronic dimensional orbital constitute the quark-mark formula for hadrons. The quark-mark formula provides the criteria for stable hadrons.

In atomic orbitals, the transition from one orbital to another orbital is through the emission or absorption of gauge boson, photon. The transitions among hadrons are also through gauge bosons, such as weak bosons, gluon, and photon. In addition to these gauge bosons, the transitions among hadrons require the addition and the subtraction of “mass blocks”. For example, the transition from proton,  $p$  (uud) to  $\Lambda^0$  (uds), is through the addition of mass blocks to  $p$ . Conversely, the transition from proton,  $\Lambda^0$  (uds) to  $p$  (uud), is through the subtraction of mass blocks from  $\Lambda^0$ .

$$\begin{aligned}
 p &\xleftarrow{\text{mass block}} \Lambda^0 \\
 \Lambda^0 &= p + \text{mass block}
 \end{aligned} \tag{27}$$

The composition of  $\Lambda^0$  is  $p + \text{mass block}$ . Such formula involving mass blocks is the mass block formula.

All hadrons, including proton and neutron, have the mass block formulas, so all hadrons share the common mass blocks. In terms of mass, the quark-mark represents hadron only approximately. The mass from the quark-mark formula is matched by the mass from the mass block formula, which represents the mass of hadron precisely.

$$M_{\text{quark-mark formula}} \approx M_{\text{mass block formula}} = M_{\text{hadron}} \tag{28}$$

All hadrons are represented by the mass block formula. Mass blocks consist of the lowest- mass quark ( $\pi_{1/2}$  and u), lepton (e), and baryons (p and n). The mass block formula is parallel to MacGregor-Akers constituent quark model [4], whose calculated masses and

the predicted properties of hadrons are in very good agreement with observations. In the constituent quark model, the mass building blocks are the "spinor" (S with mass 330.4 MeV) and the mass quantum (mass = 70MeV). For the mass block formula, S, corresponds to u quark with the lowest mass (330.77 MeV), which is designated as U mass block. The basic quantum is the pseudoscalar quark,  $\pi_{1/2}$  (mass = 70.025 MeV), which is denoted as m mass block. The mass of MM1 is 425MeV, which is close to six m's (420MeV), so six m's appear together as a group that is denoted as X, which is not a fundamental mass block.

In addition to U and m, the mass block formula includes P (positive charge) and N (neutral charge) with the masses of proton and neutron. As in the constituent quark model, the mass associated with positive or negative charge is the electromagnetic mass, 4.599 MeV, which is nine times the mass of electron. This mass (nine times the mass of electron) is derived from the baryon-like electron that represents three quarks in a baryon and three electrons in  $d_6$  quark as in Table 2. This electromagnetic mass is the baryonic electromagnetic mass. This electromagnetic mass is observed in the mass difference between  $\pi^0$  ( $m_2$ ) and  $\pi^+$  ( $m_2+$ ) where + denotes positive charge. The calculated mass different is one electromagnetic mass, 4.599 MeV, in good agreement with the observed mass difference, 4.594 MeV, between  $\pi^0$  and  $\pi^+$ . For  $\tau$ , the difference between the calculated mass (1786 MeV) by the Barut lepton mass formula and the observed mass ( $\approx$ 1777 MeV) is about 9 MeV, which is twice of the baryonic electromagnetic mass, caused by the contribution of  $\tau$  to the baryon formation. (The values for observed masses are taken from "Particle Physics Summary "[15].) The particles in the mass block formula are listed in Table 4.

**Table 4.** Mass blocks in the mass block formula

Blocks	m	X*	U	N	P	Electromagnetic mass
Origins in quarks	$\pi_{1/2}$	$6\pi_{1/2}$	u quark	n	p	$9e$
Mass (MeV)	70.0254	420.2	330.77	939.565	938.272	4.599

\*X is MM1, which is not a fundamental mass block

The mass block formula can be represented by two different formulas: the initial mass block formula and the decay mass block formula. The initial formula is the initial match to the quark-mark formula. The initial formula reflects the structure of quark-mark formula. The decay formula is the match to the decay mode. The dominated fraction of the decay modes typically reflects the most stable hadron and the most favorable decay path. The decay mass block formula consists of the largest hadron in the dominated fraction and mass blocks.

In some cases, the initial formulas are identical to the decay formula. For example, in terms of quark-mark formula,  $\Lambda^0$  (uds) is  $p$  (uud) + BM0, representing the transition of u quark to s quark. This quark-mark formula is matched by the initial formula,  $pm_3e$ , which means  $p$  + three  $m$ 's +  $e$ . The initial formula is identical to the decay formula that represents  $p$  in the dominated fraction of decay mode. In some cases, the initial formula is not same as the decay formula. For example, in terms of the quark-mark formula,  $\Sigma^+(1385)$  (uus) is  $\Sigma^+ + BM0$ , representing the transition from  $J^P = 1/2^+$  to  $J^P = 3/2^+$ . This quark-mark formula is matched by the initial formula,  $\Sigma^+ m_3$ . The decay formula is  $\Lambda^0 m_4 e$ , where the dominated decay mode involves  $\Lambda^0$ . The calculated masses by the initial formula and the decay formula are 1384.8 MeV and 1385.7 MeV, respectively, comparing the observed mass of 1382.8 MeV. In few cases, the only mass block formula is the initial mass block formula. For example, the mass block formula for  $n$  is  $U_3$ . There is no decay formula that can calculate the mass of  $n$ . Such cases involve  $U$ .

Hadrons are the composites of mass blocks as molecules composing of atoms. As atoms are bounded together by chemical bonds, mass blocks are bounded by "hadronic bonds," connecting the mass blocks in the mass block formula. These hadronic bonds are similar to the hadronic bonds in the constituent quark model.

The hadronic bonds are the overlappings of the auxiliary dimensional orbitals. From Eq (21), the energy for the auxiliary orbital for  $U$  (u quark) is

$$\begin{aligned} E_a &= (3/2) (3 M_\mu) \alpha_w \\ &= 14.122 \text{ MeV} \end{aligned} \quad (29)$$

The auxiliary orbital is a charge - dipole interaction in a circular orbit as described by A. O. Barut [1], so a fermion for the circular orbit and an electron for the charge are embedded in this hadronic bond. The fermion for the orbital is the supersymmetry fermion for the auxiliary dimensional orbital according to Eq (5).

$$M_f = E_a \alpha_w \quad (30)$$

The binding energy (negative energy) for the bond ( $U-U$ ) between two  $U$ 's is twice of 14.122 MeV minus the masses of the supersymmetry fermion and electron.

$$\begin{aligned} E_{U-U} &= -2 (E_a - M_f - M_e) \\ &= -26.384 \text{ MeV} \end{aligned} \quad (31)$$

It is similar to the binding energy (-26 MeV) in the constituent quark model. An example of  $U-U$  bond is in neutron ( $U - U - U$ ) which has two  $U - U$  bonds. The mass of neutron can be calculated as follows.

$$\begin{aligned} M_n &= 3M_U + 2E_{U-U} \\ &= 939.54 \text{ MeV}, \end{aligned} \quad (32)$$

which is in excellent agreement with the observed mass, 939.57 MeV. The mass of proton is the mass of neutron minus the mass difference (three times of electron mass =  $M_{3e}$ ) between u and d quark as shown in Table 2. Proton is represented as  $U - U - (U - 3e)$ . The calculation of the mass of proton is as follows.

$$\begin{aligned}
 E_a \text{ for } (U-3e) &= (3/2) (3 (M_u - M_{3e})) \alpha_w \\
 M_f &= E_a \alpha_w \\
 M_p &= 2 M_U + M_{(U-3e)} + E_{U-U} + E_{U-(U-3e)} \\
 &= 938.21 \text{ MeV}
 \end{aligned} \tag{33}$$

The calculated mass is in a good agreement with the observed mass, 938.27 MeV.

The binding energy for  $m - m$  ( $\pi_{1/2} - \pi_{1/2}$ ) bond can be derived in the same way as Eqs (29), (30), and (31).

$$\begin{aligned}
 E_a &= (3/2) M_m \alpha_w \\
 M_f &= E_a \alpha_w \\
 E_{m-m} &= -2 (E_a - M_f - M_e) \\
 &= -5.0387 \text{ MeV}
 \end{aligned} \tag{34}$$

It is similar to the binding energy (-5 MeV) in the constituent quark model. An example for the binding energy of  $m - m$  bond is in  $\pi^0$ . The mass of  $\pi^0$  can be calculated as follows.

$$\begin{aligned}
 M_{\pi^0} &= 2 M_m + E_{m-m} \\
 &= 135.01 \text{ MeV}.
 \end{aligned} \tag{35}$$

The calculated mass of  $\pi^0$  is in excellent agreement with the observed value, 134.98 MeV. There is one  $m - m$  bond per pair of  $m$  's, so there are two  $m - m$  bonds for 4  $m$  's, and three  $m - m$  bonds for 6  $m$  's.

Another bond is  $N - m$  or  $P - m$ , the bond between neutron or proton and  $m$ . Since  $N$  is  $UUU$ ,  $N - m$  bond is derived from  $U - m$ . The binding energy of  $U - m$  is the average between  $U - U$  and  $m - m$ .

$$E_{U-m} = 1/2 (E_{U-U} + E_{m-m}) \tag{36}$$

An additional dipole ( $e^+e^-$ ) is needed to connect  $U - m$  to neutron.

$$\begin{aligned}
 E_{N-m} &= E_{U-m} + 2 M_e \\
 &= -14.689 \text{ MeV}.
 \end{aligned} \tag{37}$$

It is similar to -15 MeV in the constituent quark model. An example for  $N-m$  is  $\Sigma^+$  which is represented by  $pm_4$  whose structure is  $m_2 - p - m_2$ . The 4  $m$  's are connected to  $p$  with two  $N-m$  bonds. The mass of  $\Sigma$  is as follows.

$$\begin{aligned}
 M_{\Sigma^+} &= M_n + 4 M_m + 2 E_{N-m} \\
 &= 1189.0 \text{ MeV}.
 \end{aligned}$$

The observed mass is 1189.4 MeV.

N-m bond can be generalized for the transformations of all baryons. The numbers of N-m bond is quantized by  $J^P$  and the type of quarks during the baryonic transformation as follows.

**Table 5:** Quantized N-m bond

	number of N-m bonds
<u>change <math>J^P</math></u>	
$1/2^+ \rightarrow 3/2^+$	+ 1
$1/2^+ \rightarrow 1/2^-$	0
$1/2^+ \rightarrow 3/2^-$	- 1
<u>change quark</u>	
$u/d \rightarrow s$ at $J^P = 1/2^+$	+ 2
$s \rightarrow c$	+ 1
$c \rightarrow b$	+ 1

There is N – N hadronic bond between two N's. N has the structure of U – U – U. N – N has a hexagonal structure shown in Fig. 17.

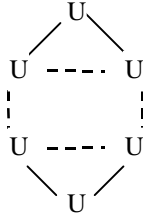


**Fig. 17:** The structure of N - N

There are two additional U – U for each N. The total number of U – U bonds between two N's is 4. An example is  $J/\psi$  ( $c\bar{c}$ ) has the mass block formula of  $N_2U_4$  with the structure. The mass of  $J/\psi$  can be calculated as follows.

$$\begin{aligned} M_{J/\psi} &= 2M_N + 4M_U + 4 E_{U-U} \\ &= 3096.7 \text{ MeV} \end{aligned}$$

The calculated mass for  $J/\psi$  is in a good agreement with the observed mass (3096.9 MeV).

Among the particles in the mass block formula, there are hadronic bonds, but not all particles have hadronic bonds. In the mass block formula, hadronic bonds appear only among the particles that relate to the particles in the corresponding quark-mark formula. The unrelated particles have no hadronic bonds. In the mass block formula, for baryons other than p and n, the core particles are P, N, and m. For the mesons consisting of u and d quarks, the core particles are m, U, and N. For the mesons containing one u, d, or s along

with s, c, or b, the core particles are U and N, and no hadronic bond exist among m's. For the mesons (c  $\bar{c}$  and b  $\bar{b}$ ), the only hadronic bond is N – N. The occurrences of hadronic bonds are listed in Table 6.

**Table 6.** Hadronic bonds in hadrons

	U – U	m – m	N(P) – m	N – N
Binding energy (MeV)	-26.384	-5.0387	-14.6894	2 U–U per N
Baryons other than n and p			√	√
Mesons with u and d only	√	√		√
Mesons containing one u, d, or s along with s, c, or b c $\bar{c}$ or b $\bar{b}$ mesons	√			√

An example is the difference between  $\pi$  and  $f_0$ . The decay modes of  $f_0$  include the mesons of s quarks from K meson. Consequently, there is no m-m for  $f_0$ . The mass block formula for  $f_0$  is  $\pi^0 X_2$ . Since  $\pi^0$  has one m-m bond, the calculation involves the subtraction of this m-m bond. The mass of  $f_0$  is as follows.

$$\begin{aligned} M &= M\pi^0 + 12 M_m - E_{m-m} \text{ from } \pi^0 \\ &= 980.3 \text{ MeV} \end{aligned}$$

The observed mass is  $980 \pm 10$  MeV.

In addition to the binding energies for hadronic bonds, hadrons have Coulomb energy (-1.2 MeV) between positive and negative charges and magnetic binding energy ( $\pm 2$  MeV per interaction) for U–U from the constituent quark model [4]. In the constituent quark model, the dipole moment of a hadron can be calculated from the magnetic binding energy. Since in the mass block formula, magnetic binding energy becomes a part of hadronic binding energy as shown in Eq (22), magnetic binding energy for other baryons is the difference in magnetic binding energy between a baryon and n or p. If a baryon has a similar dipole moment as p or n, there is no magnetic binding energy for the baryon. An example for Coulomb energy and magnetic binding energy is  $\Lambda$  (uds,  $J=1/2$ ) whose formula is  $Pm_3-$  with the structure of  $m_2-P-m_1-$  e. The dipole moment of  $\Lambda^0$  is  $-6.13 \mu_N$ , while the dipole moment of proton (P) is  $2.79 \mu_N$  [4]. According to the constituent quark model, this difference in dipole moment represents -6 MeV magnetic binding energy. The Coulomb energy between the positive charge P and the negative charge is -1.2 MeV. The electromagnetic mass for is 4.599 MeV. The mass of  $\Lambda^0$  is calculated as follows.

$$\begin{aligned} M_{\Lambda^0} &= M_p + 3M_m + M_{e.m.} + 2 E_{N-m} + E_{mag} + E_{coul} \\ &= 1116.4 \text{ MeV} \end{aligned}$$

The observed mass is  $1115.7 \pm 0.0006$  MeV.

The quark-mark formula involves both quarks and marks. The formula constitutes the approximated mass for hadrons. Table shows the quark-mark formula for some baryons.

**Table 7** : The Quark-Mark Formulas for Baryons

<u>Quark-Mark</u>	<u>MeV</u> (calculated)	<u>Baryon</u>
<u>Mark</u>		
<i>BM0</i>	176.1	$d/u \rightarrow s$ $p(udd) + BM0 \approx \Lambda^\circ(uds)$ $p(udd) + 2BM0 \approx \Xi^\circ(uss)$ $\Lambda_c^+(udc) + BM0 \approx \Xi_c^+(usc)$ $\Xi_c^+(usc) + BM0 \approx \Omega_c^0(ssc)$ $\rightarrow$ higher $J^P$ with same quarks $\Lambda_c^+(1/2^+) + BM0 \approx \Sigma_c^+(1/2^+)$
<i>BM1</i>	473.6	$\rightarrow$ higher $J^P$ with same quarks $\Xi^\circ(1/2^+) + BM1 \approx \Xi^\circ(1820)(3/2^-)$
<i>BM2</i>	938.27	$\approx p(uud)$
<i>BM3</i>	1623.5	$\approx \Omega^-(sss)$ (also $\approx s + s + s$ )
<i>BM4</i>	2589.8	$\approx \Xi_c^{'+}(usc)$ (also $u + s + c$ )
<i>BM5</i>	3905.1	not found
<i>BM6</i>	5644.7	$\approx \Lambda_b^\circ(udb)$
<u>Quark</u>	70.02	$m = \pi_{1/2}$ $\rightarrow$ higher $J^P$ with same quarks $\Sigma_c(2455)^+(1/2^+) + m \rightarrow \Sigma_c(2520)^+(3/2^+)$
	1219.5	$u + u + s \approx \Sigma^+(uus)$
	1222.6	$d + d + s \approx \Sigma^-(dds)$
	2309.8	$n(udd) + c - u \approx \Lambda_c^+(udc)$
	2685.0	$\Xi^\circ(uss) + c - u \approx \Omega^\circ(ssc)$

BM0 represents the transition from  $u/d \rightarrow s$  and transition to different  $J^P$  with the same quarks. BM1 represents the transition to different  $J^P$  with the same quarks. Another way for the transition to different  $J^P$  with the same quark is through m. BM2, BM3, BM4, and BM6 corresponding to p,  $\Omega^-$ ,  $\Xi_c^{'+}$ , and  $\Lambda_b^\circ$ , respectively. The masses of  $\Sigma^+(uus)$ ,  $\Sigma^-(dds)$ ,  $\Lambda_c^+(udc)$ ,  $\Omega_c^\circ(ssc)$  are about the masses of  $u + u + s$ ,  $d + d + s$ ,  $n(udd) + c - u$ , and  $\Xi^\circ(uss) + c - u$ , respectively.

Such quark-mark formulas can be matched with the initial mass block formulas. The initial mass block formulas in the same group can be connected together into a the initial mass block sequence. For example, for the  $\Lambda/\Xi$  group, the initial mass block sequence is as Fig. 18.

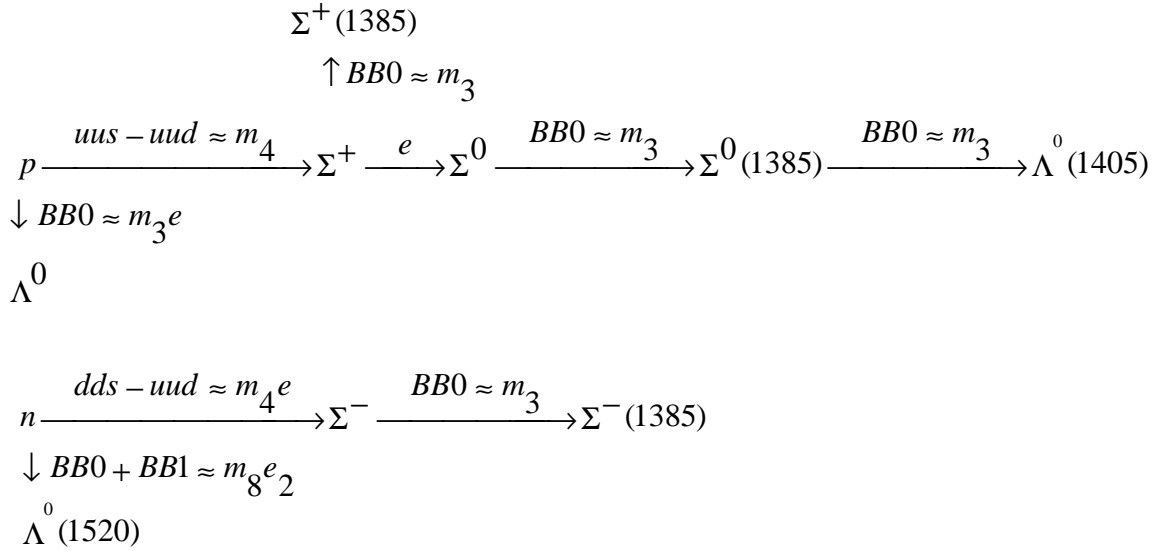


**Fig. 18:** The initial mass block sequence for  $\Lambda/\Sigma$  baryons

The decay mass block formula involves the mass blocks plus the largest baryon in the dominated fraction of decay modes. The calculated masses from the initial formula and the decay formula for the same hadron are nearly the same. Table and Table show  $I(J^P)$ , quark compositions, the initial mass block formulas derived from the quark-mark formulas, the decay mass block formulas, the calculated masses based on the decay mass block formulas, and the comparisons with the observed masses [35] for all well-defined baryons.

**Table 8.** Baryons (N,  $\Lambda/\Sigma$ ,  $\Xi^\circ$ , and  $\Lambda_c/\Sigma_c$  baryons)

Baryons	$I(J^P)$	quark	initial formula and sequence	decay formula	Calculated mass	Observed mass	Difference
<u>N-baryons</u>							
n	$1/2(1/2^+)$	udd	$U_3$	$U_3$	939.54	939.57	-0.03
p	$1/2(1/2^+)$	uud+	$BM2 = U_3^{-1/3}e$	$U_3^{-1/3}e$	938.21	938.27	-0.06
<u><math>\Lambda/\Sigma</math> baryons</u>							
$\Lambda^\circ$	$0(1/2^+)$	uds	$p + BM0 \approx pm_3e$	$pm_3e$	1116.4	1115.7	0.7
$\Sigma^+$	$1(1/2^+)$	uus+	$u + u + s \approx pm_4$	$pm_4$	1189.0	1189.4	-0.4
$\Sigma^\circ$	$1(1/2^+)$	uds	$u + d + s \approx \Sigma^+e$	$\Lambda^\circ m_2$	1193.7	1192.6	1.1
$\Sigma^-$	$1(1/2^+)$	dds-	$d + d + s \approx nm_4e$	$nm_4e$	1194.9	1197.4	-2.5
$\Sigma^+(1385)$	$1(3/2^+)$	uus+	$\Sigma^+ + BM0 \approx \Sigma^+ m_3$	$\Lambda^\circ m_4e$	1385.7	1382.8	2.9
$\Sigma^\circ(1385)$	$1(3/2^+)$	uds	$\Sigma^\circ + BM0 \approx \Sigma^\circ m_3$	$\Lambda^\circ m_4$	1381.1	1383.7	-2.6
$\Sigma^-(1385)$	$1(3/2^+)$	dds-	$\Sigma^- + BM0 \approx \Sigma^- m_3$	$\Lambda^\circ m_4e$	1385.7	1387.2	-1.5
$\Lambda^\circ(1405)$	$0(1/2^-)$	uds	$\Sigma^+ + BM0 \approx \Sigma^+ m_3$	$\Sigma^+ m_3$	1402.7	1406.0	3.3
$\Lambda^\circ(1520)$	$0(3/2^-)$	uds	$n + BM0 + BM1 \approx nm_8e_2$	$nm_8e_2$	1522.5	1519.5	3.0
<u><math>\Xi^\circ</math> baryons</u>							
$\Xi^\circ$	$1/2(1/2^+)^a$	uss	$p + 2BM0 \approx pm_6e$	$\Lambda^\circ m_3e_2$	1313.1	1314.8	-1.7
$\Xi^-$	$1/2(1/2^+)^a$	dss	$\Xi^\circ e$	$\Lambda^\circ m_3e_3$	1322.5	1321.3	1.2
$\Xi^\circ(1530)$	$1/2(3/2^+)$	uss	$\Xi^\circ + BM0 \approx \Xi^\circ m_3e_2$	$\Xi^\circ m_3e_2$	1532.9	1531.8	1.1
$\Xi^-(1530)$	$1/2(3/2^+)$	dss-	$\Xi^0(1530)e$	$\Xi^0 m_3e_3$	1536.3	1535.0	1.3
$\Xi^\circ(1820)$	$1/2(3/2^+)$	uss	$\Xi^\circ + BM1 \approx \Xi^\circ m_7$	$\Lambda^\circ m_{10}$	1830.6	1823.0	7.6
<u><math>\Lambda_c/\Sigma_c</math> baryons</u>							
$\Lambda_c^+$	$0(1/2^+)^a$	udc+	$p + c - u \approx p_2 m_8 e_3$	$p_2 m_8 e_3$	2283.9	2284.9	-1.0
$\Sigma_c^+(2455)$	$1(1/2^+)$	udc+	$\Lambda_c^+ + BM0 \approx \Lambda_c^+ m_2 e_8$	$\Lambda_c^+ m_2 e_8$	2453.3	2451.3	2.0
$\Sigma_c^0(2455)$	$1(1/2^+)$	ddc	$\Sigma_c^+(2455)e$	$\Lambda_c^+ m_2 e_9$	2456.7	2452.2	4.5
$\Sigma_c^{++}(2455)$	$1(1/2^+)^a$	uuc++	$\Sigma_c^+(2455)e$	$\Lambda_c^+ m_2 e_8$	2456.7	2452.6	4.1
$\Sigma_c^+(2520)$	$1(3/2^+)^a$	udc+	$\Sigma_c^+(2455)m$	$\Lambda_c^+ m_3 e_{10}$	2515.5	2515.9	-0.4
$\Sigma_c^0(2520)$	$1(3/2^+)^a$	ddc	$\Sigma_c^0(2455)m$	$\Lambda_c^+ m_3 e_{11}$	2518.9	2517.5	1.4
$\Sigma_c^{++}(2520)$	$1(3/2^+)^a$	uuc++	$\Sigma_c^{++}(2455)m$	$\Lambda_c^+ m_3 e_{11}$	2518.9	2519.4	-0.5
$\Lambda_c^+(2593)$	$0(1/2^-)$	udc+	$\Sigma_c^0(2520)m$	$\Lambda_c^+ m_4 e_8$	2593.4	2593.9	-0.5
$\Lambda_c^+(2625)$	$0(3/2^-)^a$	udc+	$\Lambda_c^+ + 2BM0 \approx \Lambda_c^+ m_2 e_8$	$\Lambda_c^+ m_2 e_8$	2628.5	2626.6	1.9

a =  $J^P$  that is predicted by quark model, not measured

**Table 9.** Baryons ( $\Omega$ ,  $\Xi_c$ ,  $\Omega_c$ , and  $\Lambda_b$  baryons)

Baryons	$I(J^P)$	Quark initial formula and sequence	decay formula	Calculated mass	Observed mass	Difference	
<u><math>\Omega</math> baryons</u>							
$\Omega^-$	$0(3/2^+)^a(3/2^-)^b$	sss	$BM3 \approx s + s + s$	$\Lambda^0 m_8 e_3$	1672.6	1672.5	0.1
<u><math>\Xi_c</math> baryons</u>							
$\Xi_c^+$	$1/2(1/2^+)^a(3/2^+)^b$	usc+	$\Lambda_c^+ + BM0 \approx \Lambda_c^+ m_3$	$\Xi^0 m_{17} e$	2465.8	2466.3	-0.5
$\Xi_c^0$	$1/2(1/2^+)^a(3/2^+)^b$	dsc	$\Xi_c^+ e$	$\Xi^+ m_{17} e$	2472.3	2471.8	0.5
$\Xi_c^{'+}$	$1/2(1/2^+)^a$	usc+	$BM4 = u + s + c \approx \Xi_c^+ m_6 e_6$	$\Xi_c^+ m_6 e_6$	2572.6	2574.1	-1.5
$\Xi_c^{'+}$	$1/2(1/2^+)^a$	dsc	$\Xi_c^+ e$	$\Xi^0 c m_{10} e$	2578.1	2578.8	-0.7
$\Xi_c^+(2645)$	$1/2(3/2^+)^a(1/2^+)^b$	usc+	$\Xi_c^+ + BM0 \approx \Xi_c^+ m_2 e_8$	$\Xi_c^+ m_2 e_8$	2649.4	2647.4	2.0
$\Xi_c^0(2645)$	$1/2(3/2^+)^a(1/2^+)^b$	dsc	$\Xi^0 c + BM0 \approx \Xi^0 c m_2 e_8$	$\Xi_c^0 m_2 e_7$	2646.0	2644.5	1.5
$\Xi_c^+(2790)$	$1/2(1/2^+)^a$	usc+	$\Xi_c^+ + BM0 \approx \Xi_c^+ m_3 e_2$	$\Xi_c^+ m_3 e_2$	2792.2	2790.0	2.2
$\Xi_c^0(2790)$	$1/2(1/2^+)^a$	dsc	$\Xi_c^+ + BM0 \approx \Xi_c^0 m_3$	$\Xi_c^0 m_3$	2788.9	2790.0	-1.1
$\Xi_c^+(2815)$	$1/2(3/2^-)^a(3/2^+)^b$	usc+	$\Xi_c^+ + 2BM0 \approx \Xi_c^+ m_5$	$\Xi_c^+ m_5$	2816.4	2814.9	1.5
$\Xi_c^0(2815)$	$1/2(3/2^-)^a(3/2^+)^b$	dsc	$\Xi^0 c + 2BM0 \approx \Xi_c^0 m_5$	$\Xi_c^0 m_5$	2821.9	2819.0	2.9
<u><math>\Omega_c</math> baryons</u>							
$\Omega_c^0$	$0(1/2^+)^a$	ssc	$\Xi_c^+ + BM0 \approx \Xi^0 + c - u$	$\Omega^- m_{15} e$	2696.9	2697.5	-1.1
<u><math>\Lambda_b</math> baryons</u>							
$\Lambda_b^0$	$0(1/2^+)^a(3/2^+)^b$	udb	$BM6 \approx b + 2BM0$	$\Lambda_c^+ m_{48} e$	5621.3	5624.0	-2.7

a =  $J^P$  that is predicted by quark model, not measured

b =  $J^P$  that fits the calculation

For mesons, mesonic marks are matched and replaced by mass blocks, such as X and U. MM1, MM2, MM3, MM4, MM5, MM6, and MM7 are replaced by X,  $U_3$ ,  $U_6$ ,  $U_9$ ,  $U_{16}$ ,  $U_{24}$ , and  $U_{32}$  with masses 420.1, 939.5, 1853, 2977, 4897, 7332, and 10587 MeV respectively, which are close to the original masses, 425.8, 934, 1758, 3006, 4805, 7295, 10635 MeV, respectively.

$\pi$  represents MM0. MM1 is X, and  $Xme = K^\pm$ . X is also for the transition between two different hadrons with the same quarks. U and m are also for the transition between two different hadrons with the same quarks.  $\eta'(958)$  represents MM2. MM2 is also  $U_3$ , MM2 that is one of the mass blocks in the mass block formula. K represents MM1. MM2 is  $U_3$  and  $\phi(1020) = U_3 m e_2$ , analogous to  $Xme$  for  $K^\pm$ . MM3 is  $U_6$ , and  $U_6 e_2 = D(1865)^\circ$ . Both  $\eta_c(1s)$  and  $J/\psi$  represent MM4 for  $c\bar{c}$  mesons. Possibly, due to the absence of MM6 ( $U_{24}$ ), MM5 ( $U_{16}$ ) moves toward higher mass, resulting in  $U_{17} m e_3 = B^0$  that is higher mass than  $U_{16}$ . The absence of MM6 also allows a number of stable  $\Upsilon$ 's ( $b\bar{b}$ ) below MM7. MM7 ( $U_{32}$ ) is  $\Upsilon(4s)$  that is the only  $\Upsilon$  whose decay mode is  $B^0 \bar{B}^0$  that is MM5. Table 10 shows the quark-mark formulas for mesons.

**Table 10:** The Quark-mark Formula for Mesons

<u>Quark-Mark</u>	<u>mass block</u>	MeV	<u>Mesons</u>
(calculated)			
<u>Mark</u>			
<i>MM0</i>	$m_2$	140.05	u/d with m-m bond ( $\pi = m_2$ )
<i>MM1</i>	X	420.15	$Xm Xme = K^\pm$ → different hadron with the same quarks $\pi^0 (1(0^+)) + X \rightarrow \eta (0(0^+))$
<i>MM2</i>	$U_3$	939.5	$\approx \eta '(958)$ $U_3me_2 = \phi (1020)$
<i>MM3</i>	$U_6$	1852.7	$U_6e_2 = D(1865)^0$
<i>MM4</i>	$U_9$	2976.9	$U_9 = c \bar{c}\eta_c (1s)$
	$U_4N_2$	3096.7	$U_4N_2 = J/\psi$
<i>MM5</i>	$U_{16}$	4896.6	$U_{17}me_2 = B^\pm$
<i>MM6</i>	$U_{24}$	7332	none
<i>MM7</i>	$U_{32}$	10584	$\Upsilon (4s)$ (also b + b)
<u>Quark</u>			→ different hadron with same quarks
	$m_n$	70.03 (m)	$\eta (1405) + m \rightarrow \eta (1475)$
	$U_n$	330.67 (U)	→ different hadron with the same quarks
		635.2 ( $U_2$ )	$\eta '(958) (0(0^+)) + U \rightarrow \eta (1295) ((0(0^+))$
		1008.3	$\pi^0 (1(0^+)) + U_2 \rightarrow \rho (770) (1(0^-))$
		888.8	$p + m \approx K^*(892)^\pm$
		890.3	$u + s \approx \phi (1020)$
		2031.8	$d + s \approx K^*(892)^0$
		2033.3	$u + c \approx D^*(2007)^0$
			$d + c \approx D^*(2010)^\pm$

The quark-mark formulas can be matched with the initial mass block formulas. The initial mass block formulas in the same group can be connected together into the initial mass block sequence. For example, for the unflavored group with only u/d, the initial mass block sequence is as Fig. 19.

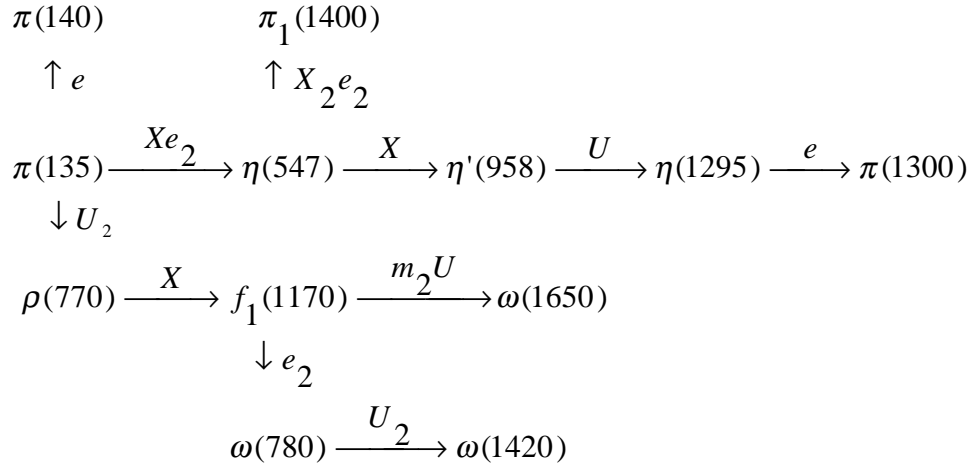


**Fig. 19:** The initial mass block sequence for the unflavored group with only u/d

Tables 11, 12, and 13 show  $I(J^P)$ , quark compositions, the initial mass block formulas derived from the quark-mark formulas, the decay mass block formulas, the calculated masses based on the decay mass block formulas, and the comparisons with the observed masses [35] for all well-defined mesons.

**Table 11.** Unflavored mesons

Meson	$I^G (J^P)$	Quark	initial formula and sequence	Decay formula	Calculated mass.	Observed mass	Difference
<u>only u, d, or lepton in decay mode</u>							
$\pi^0 (135)$	$1^- (0^+)$	u/d	MM0	$m_2$	135.0	134.98	0.04
$\pi^\pm (140)$	$1^- (0^-)$	u/d	MM0	$m_2 e$	139.6	139.57	0.04
$\eta (547)$	$0^+ (0^+)$	u/d	$\pi + MM1 \approx \pi^0 X e_2$	$\pi^0 X e_2$	548.0	547.3	0.7
$\eta' (958)$	$0^+ (0^+)$	u/d	$\pi + 2MM1 \approx MM2$	$\eta (547) X e_2$	960.3	957.8	2.5
$\eta (1295)$	$0^+ (0^+)$	u/d	$\eta' (958) U$	$\eta (547) U X e_2$	1291.1	1293.0	-1.9
$\pi (1300)$	$1^- (0^+)$	u/d	$\eta' (958) U e_2$	$\rho (770) U m_3$	1301.9	1300.0	1.9
$\rho (770)$	$1^+ (1^-)$	u/d	$\pi + d + u \approx \pi^0 U_2$	$\pi^0 (135) U_2$	770.1	771.1	-1.0
$\omega (782)$	$0^- (1^-)$	u/d	$\rho (770) e_2$	$\pi^0 (135) U_2 e_2$	778.1	782.6	-4.5
$h_1 (1170)$	$0^- (1^+)$	u/d	$\rho (770) X$	$\rho (770) X$	1176.1	1170.0	6.1
$\pi_1 (1400)$	$1^- (1^+)$	u/d	$\eta (547) X_2 e_2$	$\eta (547) X_2 e_2$	1365.4	1370.0	-4.6
$\omega (1420)$	$0^- (1^-)$	u/d	$\omega (782) U_2$	$\rho (770) U_2 e_2$	1414.3	1419.0	-4.7
$\omega (1650)$	$0^- (1^-)$	u/d	$\omega (1420) U e_2$	$\rho (770) U X m_2 e_2$	1649.9	1649.0	0.9
<u>u and d in major decay modes, s in minor decay modes</u>							
$f_0 (980)$	$0^+ (0^{++})$	u/d/s	$\pi^0 X_2$	$\pi^0 X_2$	980.3	980.0	0.3
$a_0 (980)$	$1^- (0^{++})$	u/d/s	$f_0 (980) e_2$	$\eta (547) X$	982.6	984.0	4.4
$b_1 (1235)$	$1^+ (1^+)$	u/d/s	$u + d + s \approx U_3 m_4 e_2$	$\pi^+ U_2 m_2 e$	1228.8	1229.5	-0.7
$a_1 (1260)$	$1^- (1^{++})$	u/d/s	$2MM0 + MM2 \approx$	$\pi^0 U_3 m_2 e_2$	1228.8	1230.0	-1.2
			$\eta' (958) m_4$				
$f_2 (1270)$	$0^+ (2^{++})$	u/d/s	$f_0 (980) m_4$	$\pi^0 U_2 X m e_2$	1273.3	1275.4	-2.1
$f_1 (1285)$	$0^+ (1^{++})$	u/d/s	$f_2 (1270) e_2$	$\pi^0 U_3 X m_3$	1289.6	1281.9	7.7
$a_2 (1320)$	$1^- (2^{++})$	u/d/s	$a_0 (980) U$	$\rho (770) U m_3$	1318.0	1318.0	-1.0
$\rho (1450)$	$1^+ (1^-)$	u/d/s	$a_2 (1320) m_2$	$\rho (770) U m_5 e_2$	1465.0	1465.0	0.0
$a_0 (1450)$	$1^- (0^{++})$	u/d/s	$a_0 (980) X m$	$\eta (547) X_2 m$	1472.7	1474.0	-1.3
$f_0 (1500)$	$0^+ (0^{++})$	u/d/s	$f_1 (1285) m_3 e_2$	$\pi^0 U_3 X$	1507.7	1507.0	0.7
$\omega_3 (1670)$	$0^- (3^-)$	u/d/s	$4MM1 \approx U_4 X$	$\pi^0 U_4 m_4$	1664.0	1667.0	-3.0
$\pi_2 (1670)$	$1^- (2^+)$	u/d/s	$U_4 X e_2$	$\pi^+ U_4 m_4 e_2$	1672.0	1670.0	2.0
$\rho_3 (1690)$	$1^+ (3^-)$	u/d/s	$s + s + s$	$\rho (1450) m_3 e_2$	1683.1	1691.0	-7.9
$\rho (1700)$	$1^+ (1^-)$	u/d/s	$\rho_3 (1690) e_2$	$\pi^+ U_5 e_2$	1700.9	1700.0	0.9
$\pi (1800)$	$1^- (0^+)$	u/d/s	$a_0 (1450) U$	$\pi^+ U_4 X e_2$	1808.7	1801.0	7.7
$a_4 (2040)$	$1^- (4^{++})$	u/d/s	$\omega_3 (1670) U e_2$	$\pi^+ U_6 e_2$	2005.3	2011.0	-5.7
$f_4 (2050)$	$0^+ (4++)$	u/d/s	$a_4 (2040) e_2$	$\pi^0 U_5 m_5$	2043.1	2025.0	9.1
<u>s in major decay modes</u>							
$\Phi (1020)$	$0^- (1^-)$	s/u/d	$U_3 m e_2$	$U_3 m e_2$	1017.6	1019.4	-1.8
$\eta (1405)$	$0^+ (0^+)$	s/u/d	$\Phi (1020) U m$	$K^0 (498) U_2 m_4$	1409.0	1410.3	-1.3
$f_1 (1420)$	$0^+ (1^{++})$	s/u/d	$U_3 X m$	$K^0 (498) U_2 m_4 e_2$	1421.0	1426.3	-5.3
$\eta (1475)$	$0^+ (0^+)$	s/u/d	$\eta (1405) m$	$K^0 (498) U_2 m_5$	1483.0	1476.0	7.0
$f_2 (1525)$	$0^+ (2^{++})$	s/u/d	$m_4 U_4$	$K^0 (498) U X m_4$	1528.7	1525.0	3.7
$f_0 (1710)$	$0^+ (0^{++})$	s/u/d	$f_1 (1420) m_4 e_2$	$K^* (892) U_2 m_2 e_2$	1680.5	1710.0	0.5
$\Phi (1680)$	$0^- (1^-)$	s/u/d	$f_2 (1525) m_2 e_2$	$K^0 (498) U_3 m_4$	1717.3	1680.0	3.3
$\Phi_3 (1850)$	$0^- (3^-)$	s/u/d	$U_6$	$K^0 (498) U_3 X$	1857.4	1854.0	3.4
$f_2 (2010)$	$0^+ (2^{++})$	s/u/d	$\Phi_3 (1850) m_2 e_2$	$O (1020) U_2 m_5 e_2$	2012.7	2011.0	1.7
$f_2 (2300)$	$0^+ (2^{++})$	s/u/d	$f_2 (1525) m_2 U_2$	$O (1020) U_2 X m_3 e_2$	2292.8	2297.0	-4.2
$f_2 (2340)$	$0^+ (2^{++})$	s/u/d	$f_2 (2010) U$	$O (1020) U_4 m_2 e_2$	2341.4	2339.0	2.4

**Table 12.** Strange, Charmed, and Bottom Mesons

Meson	$J^{PC}$	Quark	Initial formula and sequence	Decay formula	Calculated mass.	Observed mass	Difference e
<u>Light strange mesons</u>							
$K^\pm (494)$	$0^-$	$u \bar{s}, \bar{u}s$	$MM1me = Xme$	$Xme$	494.8	493.7	1.1
$K^\circ (498)$	$0^-$	$d \bar{s}$	$MM1 + m + e_2 \approx Xme_2$	$Xme_2$	498.2	497.7	0.5
$K^*_0 (1430)$	$0^+$	$d \bar{s}$	$K^\circ(498)m_4U_2$	$K^\circ(498)m_4U_2$	1413.0	1412.0	1.0
$K^*(892)^\pm$	$1^-$	$u \bar{s}, \bar{u}s$	$u + s \approx K^\pm (494)Um$	$K^\pm (494)mU$	894.5	891.6	2.9
$K^*(892)^\circ$	$1^-$	$d \bar{s}$	$d + s \approx K^*(892)^\pm e$	$K^*(892)^\pm e$	896.2	896.1	0.1
$K_1 (1270)$	$1^+$	$d \bar{s}$	$K^0(498)m_2U_2$	$K^0(498)U_2 m_2$	1272.9	1273.0	-0.1
$K_1 (1400)$	$1^+$	$d \bar{s}$	$K_1 (1270)m_2$	$K^*(892)^\circ Xme_2$	1394.3	1402.0	-7.7
$K^*(1410)$	$1^-$	$d \bar{s}$	$K^\circ(498)m_4U_2$	$K^\circ(498)U_2m_4$	1413.0	1414.0	-1.0
$K^*_{2(1430)}^\pm$	$2^+$	$u \bar{s}, \bar{u}s$	$K_1 (1270)m_2 e$	$K^0(498)U_2m_4e_3$	1424.4	1425.6	-1.2
$K^*_{2(1430)}^0$	$2^+$	$d \bar{s}$	$K^*_{2(1430)}^\pm e$	$K^0(498)U_3$	1437.2	1432.4	-4.6
$K^*(1680)$	$1^-$	$d \bar{s}$	$K^0(498)m_4U_3$	$K^0(498)U_3m_4$	1717.3	1717.0	0.3
$K_2 (1770)$	$2^-$	$d \bar{s}$	$K^*_{2(1430)}^0 Ue_2$	$K^*_{2(1430)}^0 Ue_2$	1771.2	1773.0	-1.8
$K_3^* (1780)$	$3^-$	$d \bar{s}$	$K_2 (1770) e_2$	$K^0(498)U_2Xm_3e_2$	1771.1	1776.0	-4.9
$K_2 (1820)$	$2^-$	$d \bar{s}$	$K_1 (1400)X$	$K^0(498)U_4me_2$	1816.0	1816.0	3.7
$K_4^* (2045)$	$4^+$	$d \bar{s}$	$K_3^* (1780) m_4$	$K^0(498)U_5$	2046.0	2045.0	1.0
<u>Charmed strange mesons</u>							
$D_s^\pm$	$0^-$	$s \bar{c}, \bar{s}c$	$K_2 (1820)m_2 e$	$K^0(498)U_4m_3e_2$	1968.3	1968.5	-8.6
$D_s^* \pm$	$1^-$	$s \bar{c}, \bar{s}c$	$D_s^\pm m_2$	$D_s^\pm m_2$	2108.4	2112.1	-3.7
$D_{s1}(2536)^\pm$	$1^+$	$s \bar{c}, \bar{s}c$	$D_s^* \pm X$	$D^* (2007)Um_3$	2535.4	2535.4	12.1
$D_{sJ}(2573)^\pm$	$2^+$	$s \bar{c}, \bar{s}c$	$D_s^* \pm m_2 U$	$D^0U_2m_3$	2569.7	2572.4	-2.7
<u>Charmed mesons</u>							
$D(1865)^\circ$	$0^-$	$u \bar{c}$	$MM3 \approx U_6 e_2$	$U_6 e_2$	1860.7	1864.5	-3.8
$D(1869)^\pm$	$0^-$	$d \bar{c}, \bar{d}c$	$D(1864)^\circ e$	$U_6 e_3$	1864.1	1869.3	-5.2
$D^* (2007)^\circ$	$1^-$	$u \bar{c}$	$u + c \approx D^* (1864)^\circ m_2$	$D^0 m_2$	2004.6	2006.7	-2.1
$D^* (2010)^\pm$	$1^-$	$d \bar{c}, \bar{d}c$	$d + c \approx D^* (2007)^\circ e$	$D^0 m_2 e$	20009.1	2010	-0.9
$D_1 (2420)^\circ$	$1^+$	$u \bar{c}$	$D^* (2010)^\pm X$	$D^* (2010)^\pm Ue$	2415.4	2422.2	-6.8
$D_2^* (2460)^\circ$	$2^+$	$u \bar{c}$	$U_8$	$U_8$	2461.5	2458.9	2.6
$D_2^* (2460)^\pm$	$2^+$	$d \bar{c}, \bar{d}c$	$U_8 e$	$U_8 e$	2466.1	2459	7.1
<u>Bottom mesons</u>							
$B^\pm$	$0^-$	$u \bar{b}, \bar{u}b$	$MM5Um \approx mU_{17} e_2$	$mU_{17} e_2$	5279.0	5279.0	0.0
$B^\circ$	$0^-$	$d \bar{b}$	$B^\pm e$	$mU_{17} e_3$	5282.4	5279.4	3.0
$B^*$	$1^-$	$d \bar{b}$	$MM5 X \approx XU_{16} e_2$	$B^0 e_{12}$			
				$XU_{16} e_2$	5324.7	5325	-0.3
$Bs$	$0^-$	$s \bar{b}$	$B^* me_2$	$D_s^\pm U_9Xm_3$	5364.4	5369.6	-5.2

**Table 13:**  $c\bar{c}$  mesons and  $b\bar{b}$  mesons

Meson	$J^{PC}$	Quark	Initial formula and sequence	Decay formula	Calculated mass.	Observed mass	Difference
<b><math>c\bar{c}</math> mesons</b>							
$\eta_c(1s)$	$0^{-+}$	$c\bar{c}$	$MM4 \approx U_9$	$U_9$	2976.9	2979.7	-2.8
$J/\psi$	$1^{--}$	$c\bar{c}$	$MM4 \approx N_2 U_4$	$N_2 U_4$	3096.7	3096.9	-0.2
$\chi_c(1p)$	$0^{++}$	$c\bar{c}$	$c + c \approx \eta_c(1s)X e_2$	$\pi^0 U_9 m_4 e_3$	3421.0	3415.1	5.9
$\chi_{c1}(1p)$	$1^{++}$	$c\bar{c}$	$J/\psi X$	$J/\psi X$	3517.1	3510.5	6.6
$\chi_{c2}(1p)$	$2^{++}$	$c\bar{c}$	$\chi_{c1}(1p) m_2$	$J/\psi X e_{10}$	3552.2	3556.2	-4.0
$\psi_{2s}$	$1^{--}$	$c\bar{c}$	$\eta_c(1s)m_2 X e_2$	$J/\psi X m_2 e_8$	3554.7	3686.0	-1.5
$\psi(3770)$	$1^{--}$	$c\bar{c}$	$\chi_{c2}(1p)m_3$	$D^0 X_4 m_3 e_2$	3763.2	3769.9	-6.7
$\psi(4040)$	$1^{--}$	$c\bar{c}$	$J/\psi N$	$D^0 X_5 m e_2$	4043.3	4040.0	3.3
$\psi(4160)$	$1^{--}$	$c\bar{c}$	$\psi_{2s} m U$	$\pi^0 N_4 U m_2$	4158.0	4159.0	-1.0
$\psi(4415)$	$1^{--}$	$c\bar{c}$	$\chi_c(1p)U_3 e_2$	$\pi^0 N_4 U_2 m$	4418.8	4415.0	3.8
<b><math>b\bar{b}</math> mesons</b>							
$\Upsilon(1s)$	$1^{--}$	$b\bar{b}$	$N_7 U_6 X_3 e_2$	$\eta(958)U25m3e2$	9460.2	9460.3	-0.1
$\chi_{b0}(1p)$	$0^{++}$	$b\bar{b}$	$N_{10} U_3$	$\Upsilon(1s)m_5 e_{14}$	9859.2	9859.9	-0.7
$\chi_{b1}(1p)$	$1^{++}$	$b\bar{b}$	$\Upsilon(1s)X e_2$	$\Upsilon(1s)X e_2$	9888.5	9892.7	-4.2
$\chi_{b2}(1p)$	$2^{++}$	$b\bar{b}$	$\chi_{b1}(1p)e_2$	$\Upsilon(1s)X e_8$	9908.8	9912.6	-3.8
$\Upsilon(2s)$	$1^{--}$	$b\bar{b}$	$\Upsilon(1s)X m_2$	$\Upsilon(1s)X m_2$	10020.5	10023.3	-2.8
$\chi_{b0}(2p)$	$0^{++}$	$b\bar{b}$	$\Upsilon(2s)m_3$	$\Upsilon(2s)m_3$	10233.4	10232.1	-1.3
$\chi_{b1}(2p)$	$1^{++}$	$b\bar{b}$	$\Upsilon(2s)m_2 e_2 \approx U_{31}$	$\Upsilon(2s)m_2 e_2$	10241.4	10255.2	-13.8
$\chi_{b2}(2p)$	$2^{++}$	$b\bar{b}$	$\chi_{b1}(2p)e_2$	$\Upsilon(2s)m_3 e_{10}$	10268.6	10268.5	0.1
$\Upsilon(3s)$	$1^{--}$	$b\bar{b}$	$\Upsilon(2s)U$	$\Upsilon(2s) + U$	10354.1	10355.2	-1.1
$\Upsilon(4s)$	$1^{--}$	$b\bar{b}$	$b + b = MM6 \approx U_{32}$	$B^0 U 16 e_2$	10579.7	10580.0	-0.3
$\Upsilon(10860)$	$1^{--}$	$b\bar{b}$	$\Upsilon(4s)m_4$	$U32m4$	10864.7	10865	-0.3
$\Upsilon(11020)$	$1^{--}$	$b\bar{b}$	$\Upsilon(3s)U_2$	$U32Xe2$	11012.8	11019	-6.2

## 11. *QCD and the three sets of seven orbitals*

The reasons for the confinement of quarks in colorless hadrons, asymptotic freedom, and colorflavor locking in QCD [36] can be found in the three sets of seven orbitals. Essentially, auxiliary dimensional orbital explains the confinement of quarks, principal dimensional orbital accounts for asymptotic freedom, and hadronic dimensional orbital is responsible for colorflavor locking.

The confinement of individual quarks in colorless hadrons implies hidden individual quarks. Such hidden individual quark is the result of hidden auxiliary dimensional orbital, which is a part of individual quark. The hidden individual quark manifests in the observation that only particle with integral electric charge and hypercharge can exist in isolation, and individual quark with fractional electric charge and hypercharge cannot exist in isolation. Therefore, quarks can exist only as the quark composites with integral electric charges and hypercharges. The composites of quarks are hadrons, including mesons and baryons.  $B_6(\pi_{1/2})$  is the gauge boson to maintain integral electric charges and hypercharges in hadrons. This gauge boson becomes eight gluons with  $SU(3)$  that change the color charges from quarks in order to confine quarks in colorless hadrons.

Asymptotic freedom in QCD states that the coupling strength of gluons decreases with increasing temperature. In terms of principal dimensional orbital and auxiliary dimensional orbital, the increasing temperature causes the occupation of quark to shift toward simpler principal dimensional orbital. All quarks include  $d = 7$  (Fig. 14) as principal dimensional orbital, so at increasing temperature, quarks increasingly occupy  $d = 7$  principal orbital. In  $d = 7$ , the lepton is  $v_\mu$ , which has chiral symmetry, so at very high temperature, quark in  $d = 7$  has chiral symmetry, which transforms high-mass constituent quarks into low-mass current quarks. Being in principal dimensional orbital, quarks are not hidden, and do not need to couple with gluons. Thus, at very high temperature, quarks in principal dimensional orbital are free quasiparticles with little or no coupling with gluons as shown in the jet-like appearance for the production of hadrons in electron-positron annihilations at high energy.

At low temperature, QCD shows “color superconductivity”, resulting in colorflavor locking. In colorflavor locking, flavors and colors are correlated. The gluons become massive and electrically charged. The quark charges are shifted. The electric charges of these particles all become integral multiples of the charge of electron. The reason for colorflavor locking is that at decreasing temperature, the occupation of quarks shifts increasingly toward more complicate hadronic dimensional orbital. In hadronic dimensional orbital,  $B_6(\pi_{1/2})$  as gluons become massive, acquires  $\pm$  electric charge, and becomes a part of pion and other hadrons as shown in the constituent quark model. Essentially, at low temperature, QCD becomes CQD (constituent quark dynamics).

In summary, quarks start with the occupation of both principal dimensional orbital and hidden auxiliary dimensional orbital, resulting in the confinement of quarks. At increasing temperature, the occupation of quarks increasing shifts toward simpler principal dimensional orbital, resulting in asymptotic freedom. At decreasing temperature, the occupation of quarks shifts increasingly toward more complicate hadronic dimensional orbital, resulting in colorflavor locking.

## 12. Conclusion

The foundation of the cosmic evolution is the multiverse, which consists of two variable components: varying dimension number and varying object-space. Different universes in the multiverse have different variables from these two variable components. Varying dimension number consists of varying space-time and mass dimensions. The varying speed of light is quantized by varying space-time dimension, resulting in varying mass in terms of varying mass dimension. The transformation of varying mass in terms of varying mass dimension is by varying supersymmetry, relating to dimensional fermions and bosons. Four objects (string, membrane, particle, and particle-wave) and four spaces (blank space, fermion space, boson space, and detachment space) constitute varying object-space.

The evolution of our expanding universe involves four stages: the pre-universe, the pre-expanding universe, the mixed pre-expanding universe, and the expanding universe. In the pre-universe, object and vacuum take turn to exist equally at the same location. It is an

equilibrium state between vacuum and the pair of ten-dimensional superstring and anti-superstring with a non-zero vacuum energy. The vacuum fluctuation (Figs. 1, 2, 3, and 4) results in the pre-expanding universe with the chiral boundary positive charged 9-brane and the chiral boundary negative charged 9-antibrane separated by pregravity (the predecessor of gravity) and anti-pregravity. The collapse and the bounce of the pre-expanding universe result in the generation of the achiral mixed 9-particle with the multiple dimensional Kaluza-Klein structure, achiral pregravity, achiral anti-pregravity, and zero vacuum energy (Fig. 5).

The decrease in vacuum energy leads to the dimension number transformation into mixed particles with lower space-time and mass dimensions, resulting in the cosmic expansion. The two modes, the slow mode and the quick mode, of the cosmic expansion lead to two universes, the hidden universe and the observable universe, respectively. In the slow mode, the space-time and mass dimensions decrease and then increase gradually and stepwise. In the quick mode, the space-time dimension decreases to four immediately and then the stepwise fractionalization and the simultaneous fission of 4D particles change 4D particles into the 4D particles with mass dimensions from 4 to 9. The stepwise fractionalization results in the inflation, and the simultaneous fission leads to the formation of dark matter and baryonic matter with different principal dimensional orbitals. The mechanism to generate principal dimensional orbital leads to the creation of cosmic radiation and the space for quantum mechanics. After the inflation and the fission, the cooling of the universe is accomplished by the non-inflationary decelerating expansion, resulting in the big bang. The cosmic evolution involving objects and spaces is shown in Fig. 6.

In the expanding universe, the hidden universe and the observable universe are incompatible until the particles in the hidden universe are converted to the 4D particles compatible to the 4D particles in the observable universe. The compatible universes lead to the emergence of dark energy that causes accelerated cosmic expansion in the observable universe. The contraction of the hidden universe from the 4D particle to the 5D particle brings about the contraction in the observable universe. Eventually, both universes are back to the mixed pre-expanding universe to start another cycle as shown in Fig. 7.

The observable universe is the Milky Universe. In the Milky Universe model, baryonic matter with four-mass dimension is incompatible with dark matter with higher mass-dimensions. Both of them are compatible with cosmic radiation. The incompatibility increases with the increasing size of the universe. Such incompatibility brings about the formation of inhomogeneous structure (anisotropies in the CMB) where the baryonic matter domains surrounded by the dark matter halos as oil droplets surrounded by water in emulsion. The gravitational interaction between baryonic matter and dark matter can be described by the Modified Newtonian Dynamics (MOND) (Fig. 8). The five periods (Fig. 12) of baryonic structure development in the order of increasing incompatibility between baryonic matter and dark matter are the free baryonic matter, the baryonic droplet, the galaxy, the cluster, and the supercluster periods. The transition to the baryonic droplet generates density perturbation in the CMB. The transition from the baryonic droplet to galaxy is through the big eruption for the formations of the first-generation galaxies, including elliptical, normal spiral (Fig. 10), barred spiral (Fig. 11), irregular, and dwarf spheroidal galaxies. The transitions to cluster and supercluster are the mergers and interactions of galaxies for the formation of the second-generation galaxies,

including modified giant ellipticals, cD, evolved S0, dwarf elliptical, BCD, and tidal dwarf galaxies. The universe now is in the early part of the supercluster period. The whole observable expanding universe behaves as one unit of emulsion with increasing incompatibility between dark matter and baryonic matter.

The transformation of few dark matter particles inside galaxies to baryonic matter is the source of high-energy cosmic rays. The calculated values (eq. (14) and eq. (15)) for the low-energy cutoff, the knee, the ankle, and the high-energy cutoff are in agreement with the observed values.

All leptons, quarks, and gauge bosons can be placed in the periodic table of elementary particles (Table 2). As the periodic table of elements derived from atomic orbital, the periodic table of elementary particles is derived from the two sets of seven orbitals: principal dimensional orbital (Fig. 14) for gauge bosons and low-mass leptons and auxiliary dimensional orbital (fig 14) for high-mass leptons and individual quarks. (Seven orbitals come indirectly from the seven extra dimensions in eleven-dimensional space-time.) The calculated masses for gauge bosons, leptons, and quarks are listed in Table 1 and Table 3.

For hadrons as the composites of individual quarks, hadronic dimensional orbital (Fig. 15) derived from auxiliary dimensional orbital is responsible. Hadronic dimensional orbital relates to the Polazzi mass formula for stable hadrons. Quarks from auxiliary dimensional orbital and hadronic marks from hadronic dimensional orbital constitute the quark-mark formulas (Tables 7 and 10) for hadrons. The transitions among quarks are through mass blocks consisting of various basic fermions, such as  $\pi_{1/2}$ , u quark, e, p, and n. The compositions from mass blocks are the mass block formulas. The mass block formula corresponds to MacGregor-Akers constituent quark model. The quark-mark formula is matched by the mass block formula, and the mass block formula constitutes the precise composition for the mass of hadron. The mass block fermions and the calculated masses are listed for baryons in Tables 8 and 9, and for mesons are listed in Tables 11, 12, and 13. These three sets of seven orbitals explain all elementary particles and hadrons. QCD describes the different occupations of quarks in the three sets of seven orbitals at different temperatures.

The masses of elementary particles can be calculated using only four known constants: the number of the extra spatial dimensions in the eleven dimensional membrane, the mass of electron, the mass of  $Z^0$ , and  $\alpha_e$ . The calculated masses for elementary particles and hadrons are in good agreement with the observed masses. For examples, the calculated masses for the top quark, neutron, and pion are 176.5 GeV, 939.54 MeV, and 135.01 MeV in excellent agreement with the observed masses,  $174.3 \pm 5.1$  GeV, 939.57 MeV, and 134.98 MeV, respectively.

In conclusion, the cosmic evolution takes place in the multiverse, we live in the Milky Universe, and our baryonic matter follows the periodic table of elementary particles and the composition of hadrons derived from the three sets of seven orbitals. This whole picture of Nature gives rise to viable cosmology, detailed explanation of astronomy, and accurate calculation of the masses of elementary particles and hadrons.

## References

\* [chung@wayne.edu](mailto:chung@wayne.edu) P.O. Box 180661, Utica, Michigan 48318, USA

- [1] D. Chung, hep-th/0111147, D. Chung, *Speculations in Science and Technology* 20 (1997) 259; *Speculations in Science and Technology* 21(1999) 277
- [2] A.O. Barut, *Phys. Rev. Lett.* 42.(1979) 1251
- [3] Paolo Polazzi, *physics/0301074*
- [4] M.H. MacGregor, *Phys. Rev. D9* (1974) 1259; *D10*, (1974) 850, *D20*, (1979) 1616; *Nuovo Cimento A58* (1980) 159; *A103* (1990) 983; D. Akers, *Int'l J. Theor. Phys.* 33 (1994) 1817; *hep-ph/0303139*, *hep-ph/0303261*, and *hep-ph/0311031*
- [5] G. Amelino-Camelia, *Int. J. Mod. Phys. D11* (2002) 35 [*gr-qc/0012051*]; *Phys. Letts. B510* (2001) 255 [*hep-th/0012238*]; J Barrow, *gr-qc/0211074*; G. Ellis and J. Uzan, *gr-qc/0305099*; J. Magueijo, *astro-ph/0305457*
- [6] A. Albrecht and J. Magueijo, *Phys. Rev. D59*, 043516 [*astro-ph/9811018*]; J. D. Barrow, *Phys. Rev. D59*, 043515 (1999); J. D. Barrow, *Phys.Lett. B564*, 1 (2003) [*gr-qc/0211074*]
- [7] R. R. Caldwell, *Phys. Lett. B* 545 (2002) 23 [*astro-ph/9908168*]; G.W. Gibbons, DAMTP-2003-19 [*hep-th/0302199*]; A. Yurov, [*astro-ph/0305019.*]; J. D. Barrow *Class.Quant.Grav.* 21 (2004) L79 [*gr-qc/0403084*]; Z-K Guo, Y-S Piao, and Y-Z Zhang, *Phys.Lett. B594* (2004) 247 [*astro-ph/0404225*]; B.Feng, M. Li, Y-S Piao, X. Zhang [*astro-ph/0407432.pdf*]
- [8] L. Randall and R. Sundrum, *Nucl. Phys. B557* (1999) 79; *Phys. Rev. Lett.* 83 (1999) 3370 ; *Phys. Rev. Lett.* 83 (1999) 4690
- [9] P. Horava and E. Witten, *Nucl. Phys. B475* (1996) 94 [*hep-th/9603142*].
- [10] J. Khoury, B. A. Ovrut, P. J. Steinhardt, and N. Turok, *hep-th/0103239*
- [11] G. Dvali and S. Tye, *Phys. Lett. B450*, (1999) 72; C. P. Burgess, M. Majumdar, D. Nolte, F. Quevedo, G. Rajesh, and R. J. Zhang, *JHEP* 0107 (2001) 047; N. Barnaby and J. Cline, *Phys.Rev. D70* (2004) 023506
- [12] J. Khoury, B. A. Ovrut, N. Seiberg, P. J. Steinhardt, and N. Turok, *Phys. Rev. D65* (2002) 086007; J. Khoury, P. J. Steinhardt, and N. Turok, *Phys. REv. Lett.* 92 (2004) 031302.
- [13] A. H. Guth, *Phys. Rev. D* 23, 347 (1981); A. D. Linde, *Phys. Lett. B108* (1982) 389; A. Albrecht and P. J. Steinhardt, *Phys. Rev. Lett.* 48 (1982) 1220.
- [14] M. Rees, *Phil.Trans.Roy.Soc.Lond.* 361 (2003) 2427
- [15] R. H. Bradenberger, *astro-ph/0208103*
- [16] A. C. S. Readhead et al *astro-ph/0402359*; Rafael Rebolo et al *astro-ph/0402466*
- [17] M. Milgrom, *New Astron.Rev.* 46 (2002) 741-753 [*astro-ph/0207231*], *astro-ph/0112069*; R. H. Sanders and S. McGaugh *astro-ph/0204521*
- [18] F. Combes, *astro-ph/0206126*
- [19] R. Barkana and A. Loeb, *astro-ph/0209515*
- [20] B. M. Tinsley and J. E. Gunn *ApJ* 203 (1976) 52
- [21] C. Conselice, *astro-ph/0212219*
- [22] B. M. Poggianti, *astro-ph/0210233*, S. F. Helsdon and T. J. Ponman, *astro-ph/0212047*

- [23] S. Leon, J. Braine, P. Duc, V. Charmandaris, and E. Brinks, astro-ph/0208494, astro-ph/0210014
- [24] M. Bonamente, M. Joy, and R. Liu, astro-ph/0211439
- [25] J. Einasto, G. Hutsi, M. Einasto, E. Saar, D. L. Tucher, V. Muller, P. Heinamaki, and S. S. Allam, astro-ph/0212312
- [26] M. J. West, astro-ph/9709289
- [27] K. Miuchi et al, Astropart. Phys. 19, 135 (2003) [ astro-ph/ 0204411]; CDMS Collaboration, Phys.Rev. D68, 082002 (2003) [hep-ex/0306001]
- [28] J. D. Anderson et al, Phys.Rev. D65, 082004 (2002) [gr-qc/0104064]
- [29] D. J. Bird et al, ApJ 441, 144 (1995)
- [30] G. L. Alberghi, K. Goldstein, D. A. Lowe Phys.Lett. B578, 247 (2004) [astro-ph/0307413]; M. Kachelriess, D.V. Semikoz Phys.Lett. B577, 1 (2003) [astro-ph/0211327]
- [31] A.D.Erlykin, A.A.Lagutin, and A.W.Wolfendale, Astropart.Phys. 19,351 (2003) [astro-ph/0209506]
- [32] P. Langacher, M. Luo, and A. Mann, Rev. Mod. Phys. 64 (1992) 87.
- [33] L. Hall, R. Jaffe, J. Rosen1985, Phys. Rep. 125 (1985) 105
- [34] C.P. Singh, Phys. Rev. D24 (1981) 2481; D. B. Lichtenberg Phys. Rev. D40 (1989) 3675
- [35] Particle data Group, (2004)
- [36] T. Schaefer, hep-ph/0304281; K. Rajagopal and F. Wilczek, hep-ph/0011333